Imaging in forensic radiology: an illustrated guide for postmortem computed tomography technique and protocols

Flach, Patricia M ; Gascho, Dominic ; Schweitzer, Wolf ; Ruder, Thomas D ; Berger, Nicole ; Ross, Steffen G ; Thali, Michael J ; Ampanozi, Garyfalia

DOI: https://doi.org/10.1007/s12024-014-9555-6

Forensic Sci Med Pathol (2014) 10:583–606
DOI 10.1007/s12024-014-9555-6

REVIEW

Imaging in forensic radiology: an illustrated guide for postmortem computed tomography technique and protocols

Patricia M. Flach · Dominic Gascho · Wolf Schweitzer · Thomas D. Ruder · Nicole Berger · Steffen G. Ross · Michael J. Thali · Garyfalia Ampanozi

Accepted: 10 March 2014 / Published online: 11 April 2014

Abstract Forensic radiology is a new subspecialty that has arisen worldwide in the field of forensic medicine. Postmortem computed tomography (PMCT) and, to a lesser extent, PMCT angiography (PMCTA), are established imaging methods that have replaced dated conventional X-ray images in morgues. However, these methods have not been standardized for postmortem imaging. Therefore, this article outlines the main approach for a recommended standard protocol for postmortem cross-sectional imaging that focuses on unenhanced PMCT and PMCTA. This review should facilitate the implementation of a high-quality protocol that enables standardized reporting in morgues, associated hospitals or private practices that perform forensic scans to provide the same quality that clinical scans provide in court.

Keywords Virtopsy · Postmortem computed tomography · PMCT · PMCTA · Protocol · Forensic imaging · Virtual autopsy

P. M. Flach (✉) · D. Gascho · W. Schweitzer · T. D. Ruder · N. Berger · S. G. Ross · M. J. Thali · G. Ampanozi
Institute of Forensic Medicine, University of Zurich, Winterthurerstrasse 190/52, 8057 Zurich, Switzerland
e-mail: patricia.flach@irm.uzh.ch

P. M. Flach · N. Berger
Institute of Diagnostic and Interventional Radiology, University Hospital Zurich, Raemistrasse 100, 8091 Zurich, Switzerland

P. M. Flach
Institute of Forensic Medicine, University of Bern, Buehlstrasse 20, 3012 Bern, Switzerland

Introduction

Postmortem cross-sectional imaging, including computed tomography (CT) and magnetic resonance imaging (MR), has been an established adjunct to forensic pathology for approximately a decade, and the number of scientific studies on postmortem imaging has increased significantly over that short time span [1–4].

The first postmortem CT (PMCT) was reported in the late 1970s in a case of fatal cranial bullet wounds [5]. This report was followed by numerous publications and even dedicated books on forensic imaging [6–14]. At the turn of the millennium, the Virtopsy project was founded at the Institute of Legal Medicine of the University of Berne in Switzerland. This project aims to establish minimally invasive routine imaging methods in the field of forensic pathology to supplement, or even obviate, traditional autopsies [15]. So far, several forensic departments worldwide have established working relationships with clinical CT or MR suites, where after-hours scans can be acquired, or they can even have dedicated CT and/or MR devices placed in their institutes to supplement, substitute or triage the daily forensic workflow [16–36]. Postmortem imaging is a new radiological subspecialty, and unlike diagnostic radiology, it does not yet have established standards.

Clinical and postmortem radiology differ significantly in several aspects [37, 38]. First, radiation is not an issue for the deceased. The imaging parameters can be adjusted to maximize image quality without safety considerations for the subject, such as the ALARA (as low as reasonably achievable) principle. Also, a body does not have motion artifacts or circulation, the latter of which is accompanied by typical postmortem sedimentation effects within the vessels or hypostasis of the lungs (inner livor mortis), sometimes obscuring image reading or even mimicking

Fig. 1 **a** Axial PMCT at the tracheal bifurcation. There is no fluid in the airways indicating aspiration. Note the diffuse ground-glass opacities in the right lung and in the dorsal parts of the left lung, corresponding to the inner livor mortis (position-dependent hypostasis in the lungs). This finding is typical of PMCT. The inner livor mortis marks depend on the position in which the person died, and the body remained. These marks provide clues as to whether the body has been moved. This body was found lying face down on the right (see Fig. 1d). The PMCT scan, however, was taken after he was already transported and stored for a while in the supine position. Therefore, there is the major settling of the hypostasis in the right (dependent) portion of the lung (due to original position) and, to a lesser degree, in the dorsal parts of the lung (due to later supine positioning). **b** Coronal MinIP (minimum intensity projection) of the airways and the lungs. The *dotted lines* indicate the predominantly right-sided, position-dependent inner livor mortis. **c** Volume rendering technique (VRT) of the lung displaying the opacified parts of the lungs due to position-dependent inner livor mortis. **d** Photograph documenting an overview of the external inspection. Note the ventral settling of the blood as a function of the body position, causing a reddish discoloration of the skin: livor mortis. The contact area of the body with the ground (or another object) on the right is spared due to the compression of the capillaries and a lack of settling of the blood. The dorsal body parts are not discolored due to the ventral and right-sided body position

real pathologies [37, 38] (Fig. 1). Second, the indications in forensic medicine are typically different from those in clinical radiology [39]. In antemortem imaging, usually specific pathologies must be ruled out or confirmed using a focused clinical protocol for a specific anatomical region. For example, chest pain indicates imaging of the thorax. Thus, clinical protocols lead to a specific diagnosis with a subsequent therapy, whereas forensic radiology's goals are to detect the cause of death and to generate insights into the deceased's mortal circumstances. However, clinical emergency or trauma scans can show the greatest resemblance to postmortem imaging, in which the investigator has only a rough idea of the suspected pathology (e.g., a traffic accident with trauma) and the imaging should detect life-threatening lesions, such as hemorrhage, internal parenchymal organ laceration and osseous or thoracic trauma,

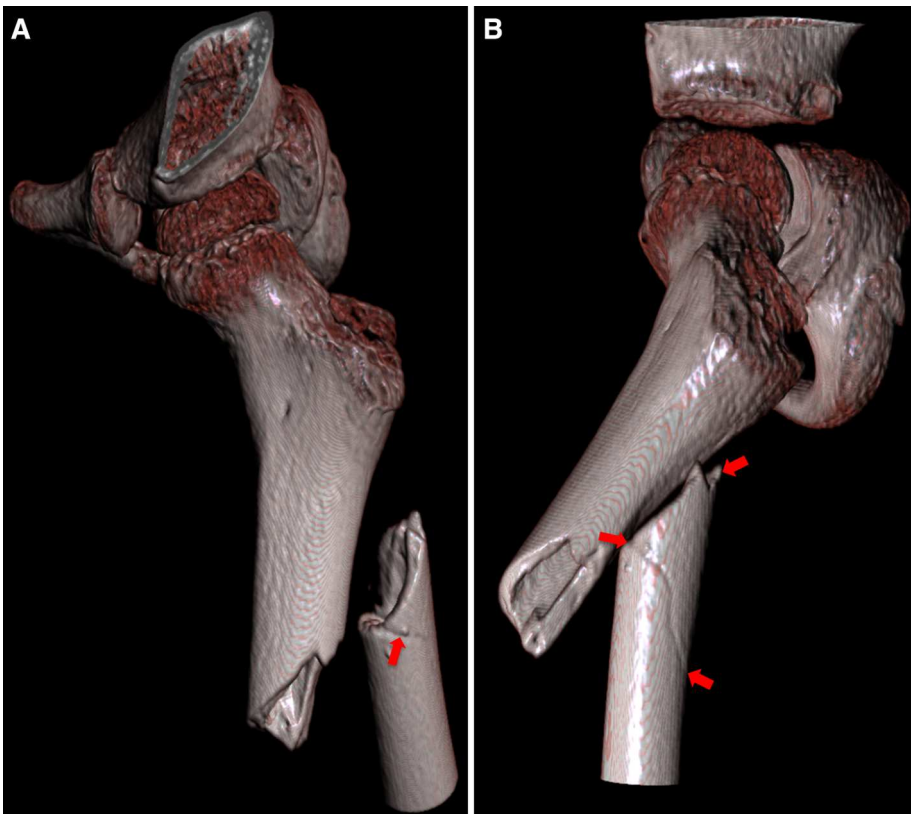

Fig. 2 **a** VRT, latero-ventral view of the proximal femur. **b** VRT, latero-dorsal view of the proximal femur. Both images, **a**, **b**, display a classic Messerer's wedge (butterfly wedge) of the fractured proximal diaphysis of the left femur (*bold red arrows*). This finding is forensically relevant, as it allows for the determination of the side of direct trauma (e.g., in a case of traffic accident reconstruction). Hence, the apex of the wedge points in the direction of force, and the base represents the impact site

from the brain to the pelvis. These techniques are similar to those in postmortem imaging for determining the cause of death [40–44].

Forensic pathology and imaging both play roles in documenting anatomy and pathology for forensic purposes. At trial, forensic imaging must sustain a technically impeccable image quality for the attorney representing the defense/victims or for the court to verify, confirm or exclude inquiries. Therefore, a technically impeccable forensic imaging protocol must be as maximally comprehensive as possible. This goal contrasts with clinical protocols, in which full or overly extensive documentation for deferred or later analysis is typically not intended, although it might be desired. Third, specific forensic considerations for postmortem imaging are different from those for clinical inquiries and include multiple objectives, such as dental identification, medical malpractice, accident reconstruction, air embolisms, reconstruction of inflicted wounds due to blunt or sharp force (Figs. 2, 3, 4), signs of intoxication, natural cause of death, identification of foreign material (Fig. 4) and homicide, to name only a few [8, 39]. Finally, forensic considerations are paramount, while postmortem imaging allows for re-evaluation, provides objective counter-expertise and serves as evidence in court. Thus, postmortem imaging must be performed using at least the same standards as clinical scans.

PMCT [and postmortem MR (PMMR)] should also include the extremities and is predominantly unenhanced, in contrast to clinical radiology. If postmortem imaging is taken a step further, the lack of cardiovascular circulation can be overcome by administering additional intravascular contrast media mixture using a roller-pump or modified heart–lung machine [45–52]. Recently described PMCT angiography (PMCTA) procedures allow for precise vascular and parenchymal localization of pathologies, which can substantially aid in forensic diagnoses. Current research on PMMR angiography (PMMRA) is scarce [53]. However, PMCTA and PMMR/PMMRA both add crucial diagnostic value to forensic imaging, although they are time-consuming and therefore have not yet been widely adopted worldwide in forensic institutions. Specific PMMR and PMMRA scanning parameters are clearly beyond the scope of this review [53–57].

In this article, we outline the main approach for a recommended standard protocol for postmortem cross-sectional imaging, focusing on unenhanced PMCT and PMCTA.

The forensic role of PMCT

Forensic indications for postmortem cross-sectional imaging can vary from institution to institution and from country to country. At our forensic institution, we use PMCT as a baseline exam, which each body delivered to the morgue undergoes, regardless of a subsequent state-

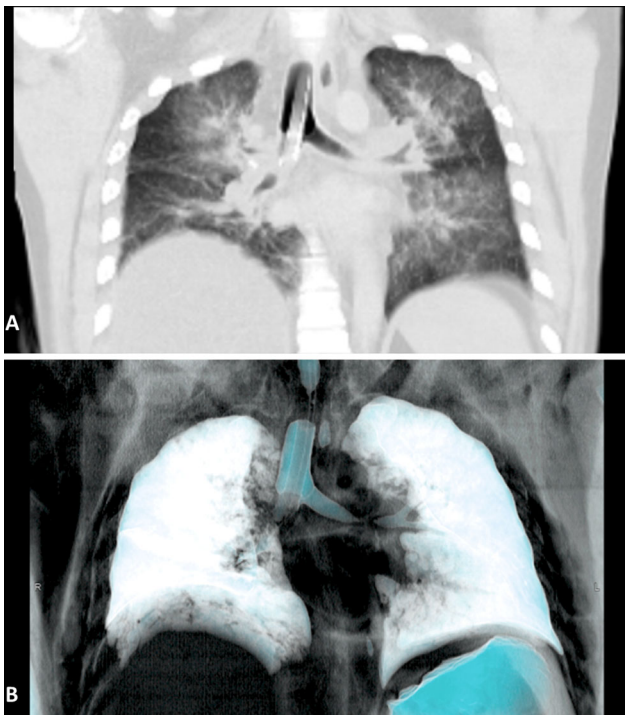

Fig. 3 **a** Coronal maximum intensity projection (MIP) of the lower airways and the lungs. Note the mal-positioned endotracheal tube in the right main bronchus. The cuff is blocked at the level of the bifurcation. These findings would have been missed during autopsy as medical devices are removed for dissection. **b** Volume rendering technique (VRT) of the air-filled structures, such as the blocked cuff of the tube, the left bronchus and the stomach (*colored in green*). The right bronchus is not ventilated due to the mal-positioned tube

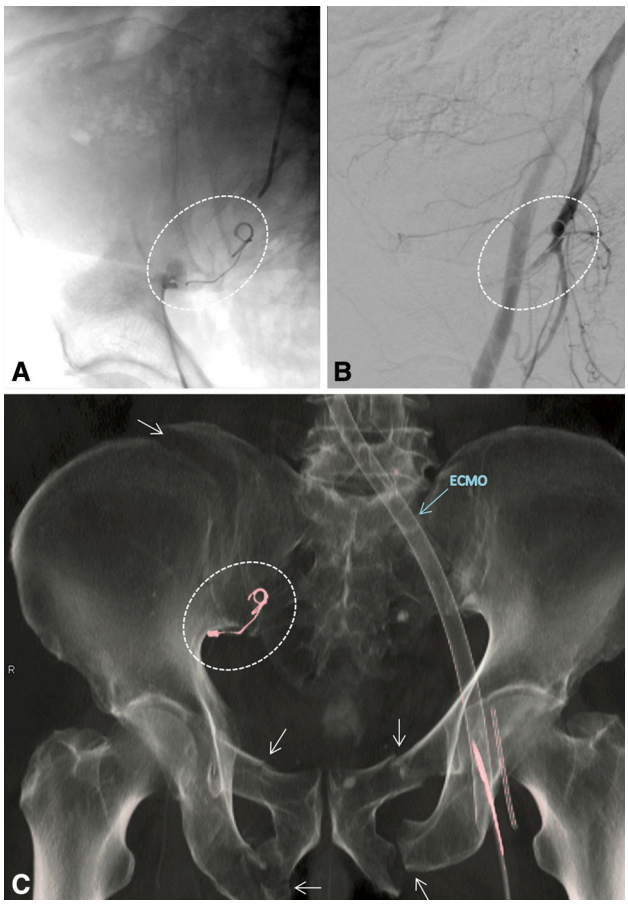

Fig. 4 **a** Antemortem conventional angiography (bone mask) with display of the coiling in the superior gluteal artery on the right. This case succumbed to extensive trauma of the pelvis (see Fig. 4c). **b** Antemortem conventional angiography, digitally subtracted to show the stopped bleeding from the largest branch of the internal iliac artery. **c** VRT PMCT of the pelvis with highlighted foreign material. The coiling (*white dotted circle*) is not impacted or misplaced. Note the line of the ECMO (extracorporal membrane oxygenation) on the left. Concomitantly, the catheters in the femoral artery and vein are correctly placed. The cause of vascular injury is the underlying extensive trauma (fractures marked with *white arrows*) to the pelvis, with SI joint dissociation and fractures of the inferior and superior pubic ramus

ordered autopsy, toxicological analysis or legal (external) inspection only. Supplementary exams, such as whole-body PMMR or focused PMMR, PMCTA or PMMRA, are based on the results of the diagnosis of the initial unenhanced PMCT, on the findings of the external inspection and on the deceased's history, in consensus between the forensic radiologist and the forensic pathologist. Additionally, all imaging is performed under a general agreement with the district attorney's office.

In other institutions, PMCT might be the only imaging modality. In these institutions, it might be used for triage purposes to reduce the sheer number of daily forensic autopsies by identifying the cases with potential unnatural causes of death for subsequent autopsy, thus obviating autopsy for natural causes of death [3, 4]. In other parts of the world, surviving family members might object to postmortem investigations, such as autopsies, out of religious or cultural motivations. In these places, the use of postmortem imaging, including PMMR, as a potential substitute to autopsy is a new approach for overcoming these problems [26, 27]. Moreover, at some institutions every fatality returning from war undergoes PMCT at a military facility to add efficiency and accuracy to the subsequent autopsy process, rather than to replace it [22–24]. Currently, some institutions primarily use postmortem imaging for scientific research purposes and not for pre-autopsy planning [58–60].

PMCT allows forensic pathologists to dissect cumbersome body parts or areas that are not routinely dissected during a standard autopsy (opening of the 3 body cavities: skull, thorax and abdomen), directed by the findings of the cross-sectional data set. These areas include the viscerocranium, shoulder girdle, extremities, outer pelvis, craniocervical junction, larynx and soft tissue of the back.

Due to this heterogeneity of imaging purposes within the domain of forensic PMCT alone, a standardized imaging

Table 1 Potential indications for PMCT

Indication	Pathology	Effect for the forensic pathologist
Self-protection	Tuberculosis, infectious diseases	Bacterial analysis, special protection during autopsy for the investigators
Medical devices	Potential medical malpractice, identification based on medical implants (prosthesis, pacemaker)	In-situ depiction and retrieval
Foreign material	Bullet, bomb fragments, sharp metal object, external or swallowed foreign material	Localization and retrieval of forensic evidence
Identification (ID)	Dental or osseous ID	ID in comparison with antemortem data
Accident reconstruction	Traumatic impact (with organ and bony lesions)	Verification of the side of potential traumatic impact, e.g., "Messerer" wedge, no maceration or extensive dissection needed
Strangulation	Laryngeal trauma, especially fractures of the hyoid or thyroid bone	Planning of autopsy procedure with focused assessment
Sharp force	Wound channel (exit and/or entry wound)	Reconstruction of inflicted wound, e.g., determining knife length/ retrieval of bullets
Blunt force	Trauma pattern, especially of osseous trauma	Reconstruction of inflicted wound, e.g., determining the inflicting instrument
Intoxication	Full bladder, tablets in stomach, drug containers in the intestines	Signs of potential intoxication with securing of evidence and toxicology
Gas embolism	Intravascular air	Determination of the extent of gas embolism and planning autopsy proof
Decomposition	In-situ depiction of remaining organs and potential pathology	In-situ depiction as during autopsy liquefied organs flow out and obscure potential pathology
Exhumation	Scanning in casket and additionally without casket as baseline exam	Baseline exam for easier assessment in this advanced stage of putrefaction or even destruction of the remains
Train fatality	3 inquiries: all body parts collected, suitable for identification (remain teeth), signs of third-party involvement, e.g., bullets in cases of body dumping	Complete collection of body parts, ID by CT feasible, exclusion of foreign material
Natural cause of death	Indirect or direct signs for natural causes of death	Baseline for potential specific exams (pmCTA, pmMR) and potential waiving of autopsy
Charred body	Potential natural cause of death before thermal impact, signs of third-party involvement, ID	Natural cause of death detectable or ID by CT feasible, ruling out of foreign material
Detection of pathologies in the "blind spots" of standard autopsy	Lesion of the viscerocranium, shoulder girdle, the extremities, the outer pelvis, the craniocervical junction, the larynx or the soft tissue of the back	Planning of autopsy procedure with potential additional dissection of routinely not dissected body parts

protocol or list of indications has remained elusive. Table 1 summarizes the potential indications for unenhanced PMCT.

General whole-body PMCT protocol

Technical considerations

The scanning device in forensic imaging should preferably feature a large bore diameter to accommodate exhumed bodies in caskets, impaled or charred bodies in fencing positions, badly decomposed and therefore bloated bodies or simply obese decedents [38, 61–63] (Fig. 5). Wide-bore CTs (with an extra space extending beyond 80 cm) can currently be purchased. However, wide-bore designs come with trade-offs, such as greater force exerted on the whirling components (X-ray tubes and detectors). A bore

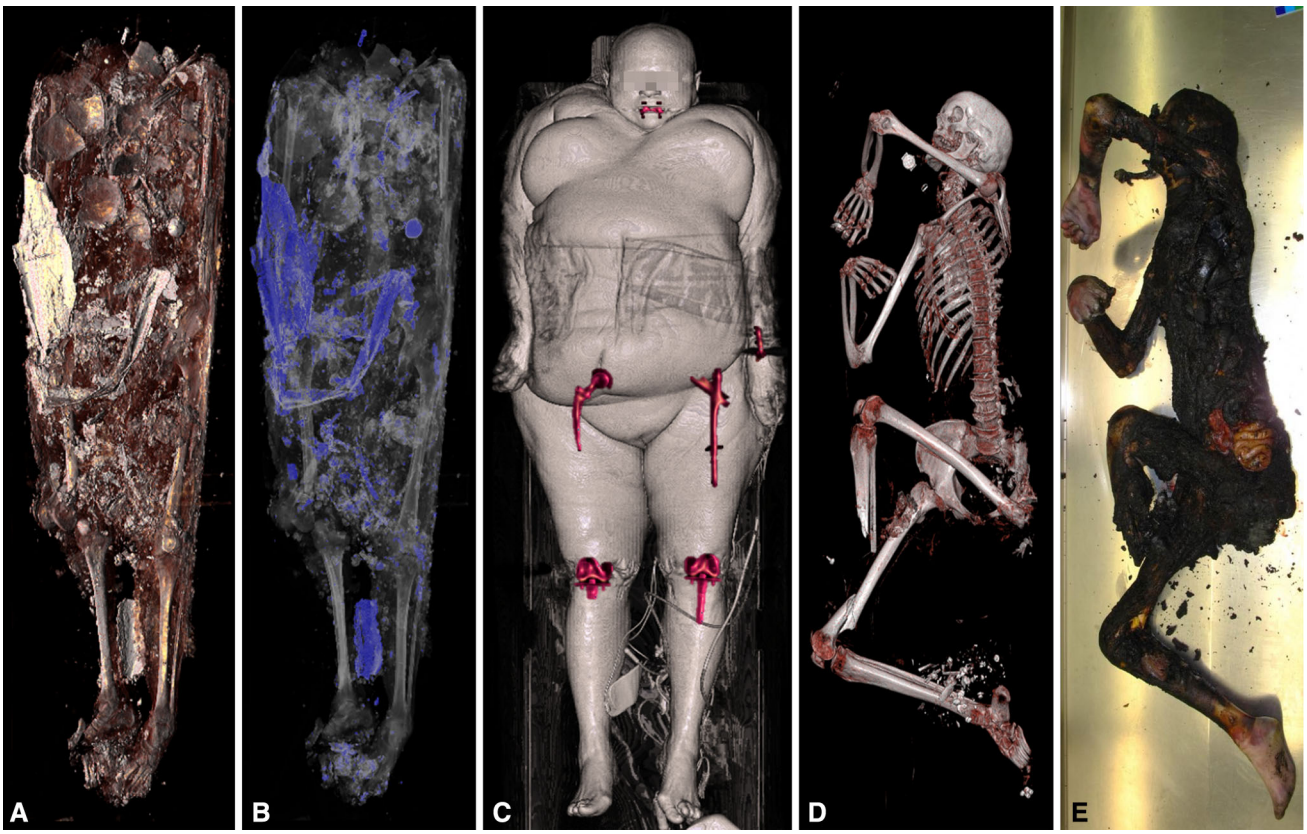

Fig. 5 **a** VRT of an exhumed body after several months of burial in the ground. Parts of the displaced skull visible in the proximal areas are obscured by significant amounts of foreign material, including soil, wood and stones. **b** The same case with *color-coded*, dense foreign material (*blue*). The bony structures are easily differentiated by this post-processing technique. **c** A very obese decedent with multiple medical implants, including total knee replacements on both sides, total hip replacement on the right, a trochanteric gamma nail with a single distal locking screw on the left, a plate osteosynthesis of the left distal radius and distinct dental work. This case clearly demonstrates the need for a large bore diameter to include as much information in the scan range as possible. **d** VRT of a charred body. This case is fixed in a distorted position that barely fits the bore due to extensive thermic destruction, although the body appears to be thin. The deceased is fragile and brittle and needs to be treated with care. Therefore, a large bore size is favorable to avoid unwanted destruction

size of 85 cm is favorable for postmortem forensic imaging. However, working with an average bore size of 78 cm is sufficient in most cases.

Body preparation

The body should be in the supine position for whole-body PMCT and should be wrapped in an artifact-free body bag (or at least in plastic foil) to diminish contamination of the CT couch. Positioning of the head with the median location of the nose is feasible to some extent by palpating the nasal bone through the body bag and repositioning the head in an orthograde position. This process clearly depends on the extent of rigor mortis. Doing so facilitates later image reconstruction and avoids the potential pitfall of mistaking the sides while reconstructing the head. The medical investigator or radiological technologist, or even the morgue technologist in charge of the PMCT scan, must ensure that the complete body is included in the scan range of the whole-body PMCT, from the vertex and the galeal soft tissue to the tips of the toes. Newer scanners allow for a scan range of up to 200 cm, and most of the deceased's body will fit. If the scan range is too short, e.g., if the decedent is taller than 2 m, bending the knees will facilitate inclusion of the whole body in one scan range. However, a drawback of this approach is that artifacts at the knees might extend the field of view (eFoV) on the data set. Alternatively, the operator can simply split the scan into 2 scan ranges and adjust the body position accordingly.

The initial whole-body PMCT should be performed without any alterations of the body; i.e., everything should be left untouched for the baseline scan, and medical devices or foreign material should not be removed (Figs. 3, 4). In high-profile cases, such as homicides, the radiological investigator must ensure that the DNA tests and criminal investigations have already been completed prior

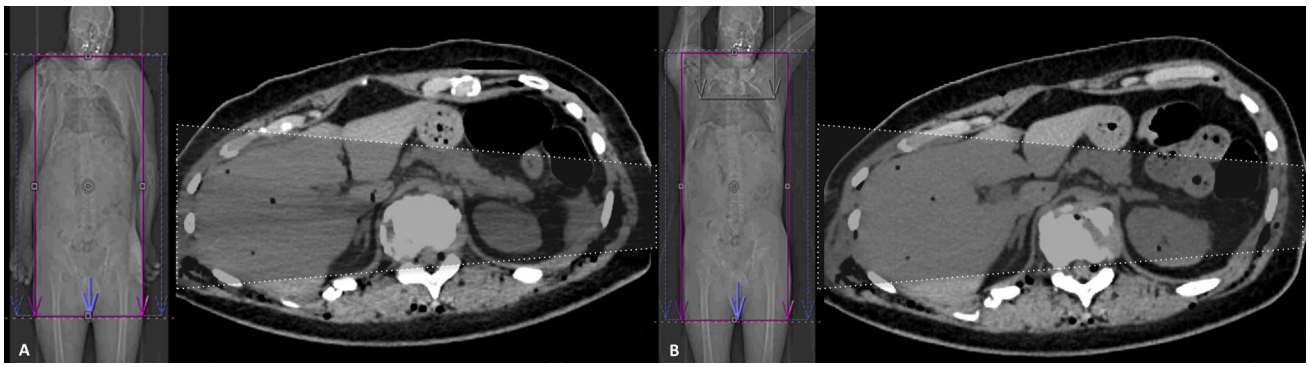

Fig. 6 **a** Omitting elevation of the arms with typical beam hardening and scatter, producing dark streaks (streak artifacts, indicated by the highlighted trapezoid) between two high attenuation objects (in this case, the bones of the lowered arms). In addition, the image quality is distinctly decreased, and a higher radiation dose is required for imaging. Thus, the arms must be elevated to obtain high-quality images and later reporting if the case goes to court. **b** This example, of the same body as in Fig. 6a, shows the substantial effect that the elevated arms have on the image quality (indicated by the *highlighted* trapezoid). Reading of the upper parenchymal organs is distinctly improved. Both images, **a**, **b**, were acquired using same imaging parameters

to the scan to avoid altering any forensic evidence from the body. When imaging dedicated body areas, external foreign material (e.g., stones, zippers, etc., but not medical devices) should be removed after the baseline scan [38].

The image quality of the torso improves, even with newer scanners, when elevating the upper extremities and fixating the wrists using a hook-and-pile fastener or simply loosely wrapping the extremities in duct tape (Fig. 6). Doing so diminishes streak artifacts in the upper abdomen, which impairs image quality and therefore poses a risk to the reporting of findings. To elevate the arms, the body bag must be opened, and rigor mortis, if present, must be broken without blunt force.

In cases of exhumation, the body should first be scanned within the casket if it fits the bore size [38] to obtain a true in situ depiction. Clearly, exhumed bodys usually show vast signs of decomposition and, therefore, potential displacement of body parts after removal from the casket. Second, a scan without the casket should follow to eliminate the artifacts from soil or stones that usually accompany exhumed coffins.

Clearly, there are cases in which the operator must abstain from elevating the arms at the expense of image quality of the torso, due to physical limitations and potential postmortem alteration of the body. The operator should avoid elevation of the upper extremities in the following scenarios (Fig. 7): (1) Decomposition: Potential detachment of the skin due to elevation of the arms, contamination of the CT couch caused by insect infestation or bodily fluids or molestation by odor (especially in clinical suites); (2) A charred body: Frequently, no alterations are feasible without concomitant destruction of the body; (3) A frozen body: The image quality will change to more hypodense parenchyma if frozen. If the body does not fit in the bore, the operator should wait until the body has defrosted; (4). Isolated trauma to the proximal upper extremity: Bending of the arms can aggravate potential fracture of the humerus or glenohumeral dislocation and create false-positive postmortem findings; (5) Vast traumatic destruction of the body (including transsection of the limbs, train fatalities or massive open trauma): Potential alteration of postmortem findings or contamination of the CT couch by bodily fluids (however, a second PMCT in ordered anatomical position of all body parts is suggested); and (6) An exhumed body: Usually adipocere and decomposition are present; therefore, the arms cannot be elevated.

Pitfalls

Postmortem fractures of the body can occur due to accidentally sloppy transfer from the gurney to the CT couch and vice versa. This pitfall is especially relevant with charred bodies. In these cases, communication with the forensic pathologist regarding the initial external inspection or later inspection during autopsy (if performed) is crucial to avoid mistaking postmortem fractures for antemortem findings. However, indirect signs of antemortem fractures, such as hematoma on PMCT or bone bruises on PMMR, might be present. Nevertheless, bone marrow edema can also occur as a result of heat-related bone changes due to thermal impact.

Postmortem fractures of the upper proximal extremity or the shoulder girdle rarely occur due to elevation of the arms. The initial whole-body PMCT without elevated arms should serve as the baseline in the latter case.

Elevation of the arms can also exclude pathologies from the scan range when the thorax and abdomen are scanned (Fig. 8) [38]. Therefore, the shoulder girdle in particular should be read on the whole-body scan (with lowered arms), and the dedicated torso scan should be read with better image quality (with elevated arms).

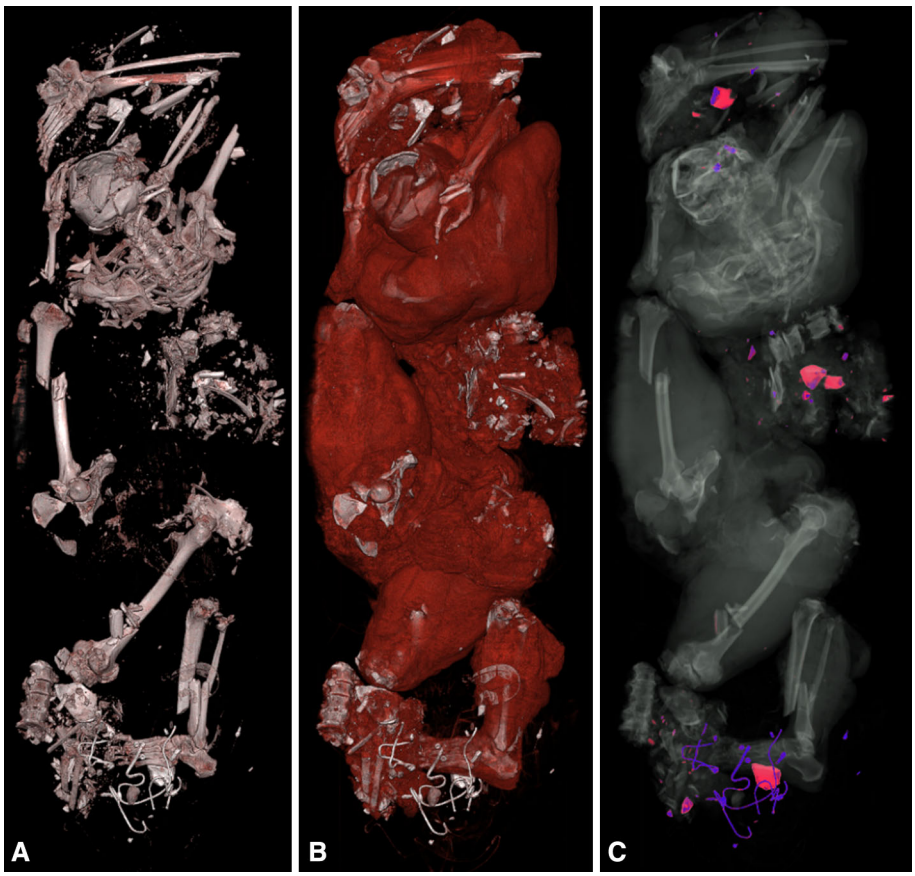

Fig. 7 **a**VRT of a train fatality with display of the bony structures. **b** VRT of a train fatality with display of the bony and soft tissue structures. **c** VRT of a train fatality with display of the bony structures, with *color-coded* dense materials, including zippers, stones, rail track gravel and dental fillings. Clearly, such cases preclude the elevation of the arms. Train fatalities with such extensive trauma pose 3 forensically relevant questions: First, are all of the body parts collected? Second, is there any sign of 3rd-party influence, such as metallic objects (e.g., projectiles), that do not belong? The train fatality might already have been dead before being hit by the train (e.g., body dumping). Third, can the body be identified? In cases with extensive trauma, the coroner should abstain from visual identification by the next of kin, which frequently is not possible. DNA analysis certainly allows for identification. However, radiological identification is less expensive and faster, if any usable antemortem radiological data are available

Whole-body PMCT (>16 multidetector CT)

Newer scanners feature longer scan ranges of almost 200 cm, and they allow for complete whole-body scans without repositioning the body. Our experience regarding the following whole-body PMCT protocol is based on a dual-source CT scanner (SOMATOM Flash Definition, Siemens, Forchheim, Germany) with 2×128 slices. Automated dose modulation (CARE Dose4D^{TM}, Siemens, Forchheim, Germany) was used for all of the scans to reduce streak artifacts. The tube voltage was 120 kV for all of the performed exams (unless otherwise stated), as the dose savings were inconsequential. The pitch factor was 0.35, and the rotation time was 0.5 s. The complete 3-step-scanning protocol is described step by step in the following section and is summarized in Table 2.

Step 1: Whole-body scan: "The Baseline"

The body is positioned using laser cross hairs to determine the exact height of the CT couch, and a line is projected onto the table, so the body is positioned exactly in the middle of the table. Small aligning lasers are also used to determine the starting point for the scout view. Folding the body bag and palpating the vertex through the body bag usually support this approach. Positioning of the head with the median location of the nose is favorable, as mentioned above. The body should be scanned head first in the supine position, with the arms at the sides or slightly crossed over the torso ("praying position") to include as much of the upper extremities in the scan field as possible.

The topogram is obtained at 120 kV and 35 mA in the anterior-posterior and lateral orientations (Fig. 9). On the

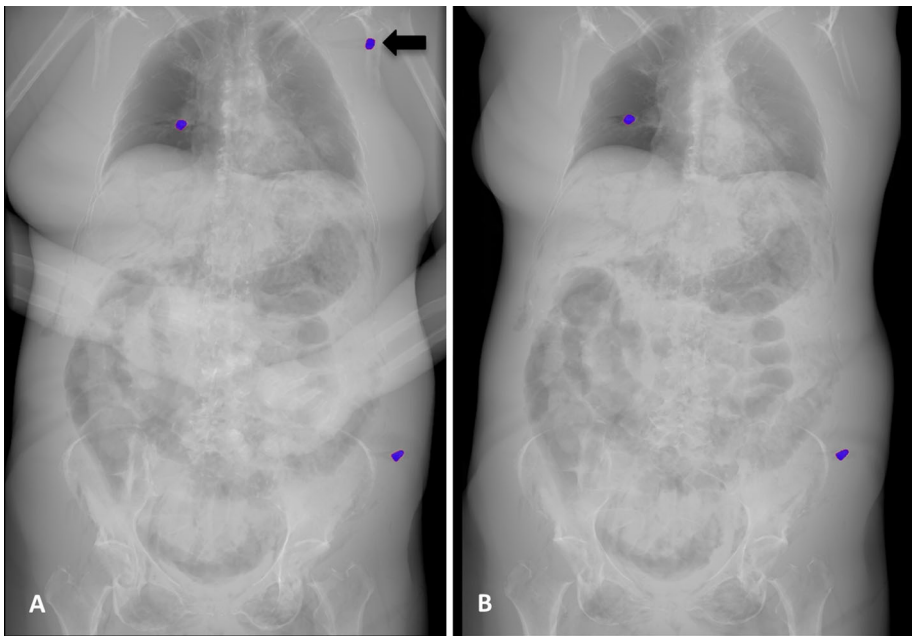

Fig. 8 **a** VRT of the torso from a homicide with lowered upper extremities. **b** VRT of the torso from a homicide with elevated arms. The left image (**a**) shows 3 projectiles (*color-coded in blue*) located within the scan range of the torso. A *black bold arrow* marks the projectile located in the left shoulder girdle. The right reconstructed image (**b**) (as well as the axial slices) displays only 2 projectiles (*color-coded in blue*) due to the elevation of the arms. Therefore, the pathology would have been missed if the image reading excluded a baseline scan with lowered arms. Moreover, the topogram-like reconstructions show an additional pneumoperitoneum and pneumomediastinum

whole-body scout image, the scan ranges from head to toe, and the whole-body scan uses a reference of 400 mA to plan the subsequent PMCT. The raw data are then reconstructed in an eFoV of 501 mm up to 780 mm (usually approximately 650 mm), to include as much of the skin surface of the body and upper limbs as possible by checking the provided box on the workstation desktop. Depending on the deceased's body mass, the complete upper extremity might or might not be included. In specific cases with external findings on the limbs, an additional extra scan of the region of interest might be required (Fig. 10).

The axial image of the whole-body is then reconstructed using the eFoV, with a slice thickness (SL) of 2 mm and an increment of 1 mm with a soft (B30) and hard (B50) kernel in the abdominal and bone window, respectively. In addition, 1 coronal whole-body reconstruction, in a soft kernel with an abdominal window using an SL of 3 mm, is also calculated (Fig. 9).

For reporting and demonstration purposes, a 360° volume rendered "movie" of the skeleton and its osseous findings is often desirable. This movie can, for example, easily display a traumatic impact on a specific side and allow for a quick overview of the extent of bony destruction in morning reports for the forensic pathologist or even in court.

Step 2: Head and neck scan

After the investigator has already ensured that the head is aligned as orthograde as feasible, the head can then be scanned with still lowered arms without any pause.

The scan ranges proximally from the vertex of the galeal soft tissue and caudally extends to the 1st thoracic vertebra (Fig. 11). Axial slices are reconstructed in a small field of view (FoV) with a maximum of 300 mm (adjustments smaller than 300 mm are favorable, the anatomy permitting) for better image quality (Fig. 12). Therefore, performing a separate head and neck scan is a necessary alternative to reconstructing the head and neck from the initial whole-body scan. Doing so minimizes streak artifacts at the base of the skull, and a smaller FoV with a special head kernel results in better image quality. Spiral images of the head and neck are acquired with an SL of 0.6 mm and an increment of 0.4 mm, in a cerebral window with a soft kernel (H31) and a bone window with a hard kernel (H60). The reference is 80 mAs with the above-mentioned automated dose modulation to reduce the artifacts from the skull base and shoulder girdle and thus the artifacts of the lower cervical spine.

The image reconstruction of the head must be orbitomeatal and symmetrically aligned for proper image reporting. The reconstruction of the acquired axial spiral includes a

Table 2 Comprehensive whole-body PMCT protocol (>16 MD–CT)

Region	Field of View	Orientation	Kernel	Window	I (mm)	SL (mm)
PMCT protocol						
Step 1: Whole-body "The Baseline"						
Whole-body	eFoV	Axial	Soft (B30)	Abdominal	1	2
Whole-body	eFoV	Axial	Hard (B50)	Osteo	1	2
Whole-body	eFoV	Coronal, 3D	Soft (B30)	Abdominal	2	3
VRT movie	360° degree, rotation on axis		Osseous preset		25 steps	
Step 2: Head and neck						
H & N	Max. 300 mm	Axial	Soft (H31)	Cerebrum	0.4	0.6
H & N	Max. 300 mm	Axial	Hard (H60)	Osteo	0.4	0.6
Head	Max. 300 mm	Axial, 3D	Soft (H31)	Cerebrum	3	4
Head	Max. 300 mm	Axial, 3D	Soft (H31)	Cerebrum	0.4	0.6
Head	Max. 300 mm	Axial, 3D	Hard (H70)	Osteo	0.4	0.6
C-spine	Small, adjusted FoV	Axial, 3D	Hard (H60)	Osteo	1	1.5
C-spine	Small, adjusted FoV	Coronal, 3D	Hard (H60)	Osteo	1	1.5
C-spine	Small, adjusted FoV	Sagittal, 3D	Hard (H60)	Osteo	1	1.5
Step 3: Thorax and abdomen						
Thorax/abdomen	Max. 500 mm	Axial	Soft (B30)	Abdomen	0.6	1
Thorax/abdomen	Max. 500 mm	Axial	Hard (B60)	Lung	0.6	1
Thorax/abdomen	Max. 500 mm	Axial	Soft (B30)	Abdomen	3	5
T-/L-spine	Small, adjusted FoV	Axial, 3D	Hard (B70)	Osteo	1	1.5
T-/L-spine	Small, adjusted FoV	Sagittal, 3D	Hard (B70)	Osteo	1	1.5
T-/L-spine	Small, adjusted FoV	Coronal, 3D	Hard (B70)	Osteo	1	1.5
Sternum	Small, adjusted FoV	Sagittal, 3D	Hard (B70)	Osteo	1	1.5
Pelvis	Small, adjusted FoV	Coronal, 3D	Hard (B70)	Osteo	1	1.5
Add-on to PMCT protocol						
Dental						
Dental	Small, adjusted FoV	Axial, 3D	Hard (U70)	Dental	0.2	0.4
Larynx						
Larynx	Small, adjusted FoV	Axial, (3D)	Medium soft (U40)	Osteo	0.2	0.4
VRT movie	360° degree, rotation on axis		Osseous preset		25 steps	

eFoV extended field of view, *I* increment, *SL* slice thickness, *3D* 3-dimensional, angulated reconstruction, *VRT* volume rendering technique, *H & N* head and neck, *C-spine* cervical spine, *T-/L-spine* thoracic and lumbar spine

thick-sliced (4 mm, increment 3 mm) stack with a cerebral window in a soft kernel (H31) via a 3-dimensional reconstruction tool for multiplanar reconstruction, which usually comes with the operating controls of the CT scanner. In addition, the thin slices of the head (SL 0.6 mm, increment 0.4 mm) are aligned with the same parameters used for the thick slices, with an osseous window in a sharp kernel (H60). The reconstruction of the head images includes the soft tissue from the vertex down to the chin (Fig. 11).

The neck reconstruction parameters are calculated in the 3-dimensional application as follows: for the axial images of the cervical spine, the FoV is minimized and properly aligned to the facet joint on both sides and to the intervertebral disk. The axial, sagittal, and coronal images of the cervical spine are all obtained with an SL of 1.5 mm and increment of 1 mm, with a bone window in a sharp kernel (H60). The reconstruction includes the occipital condyles proximally and distally the 1st thoracic vertebra (Fig. 13).

The sagittal image reconstruction is centered and aligned to the dens, and it includes the very tips of the transverse processes on both sides. The coronal images are aligned with the facet joints/dens and include the complete vertebrae on the anterior and the complete spinous process on the posterior (Fig. 13).

Step 3: Thorax and abdomen scan

According to the above-mentioned protocol, the arms are then elevated to ensure proper image quality of the torso. The FoV is usually adjusted to a width of 300–400 mm, according to the decedent's habitus; the maximum FoV should not exceed 500 mm. The scan range includes the

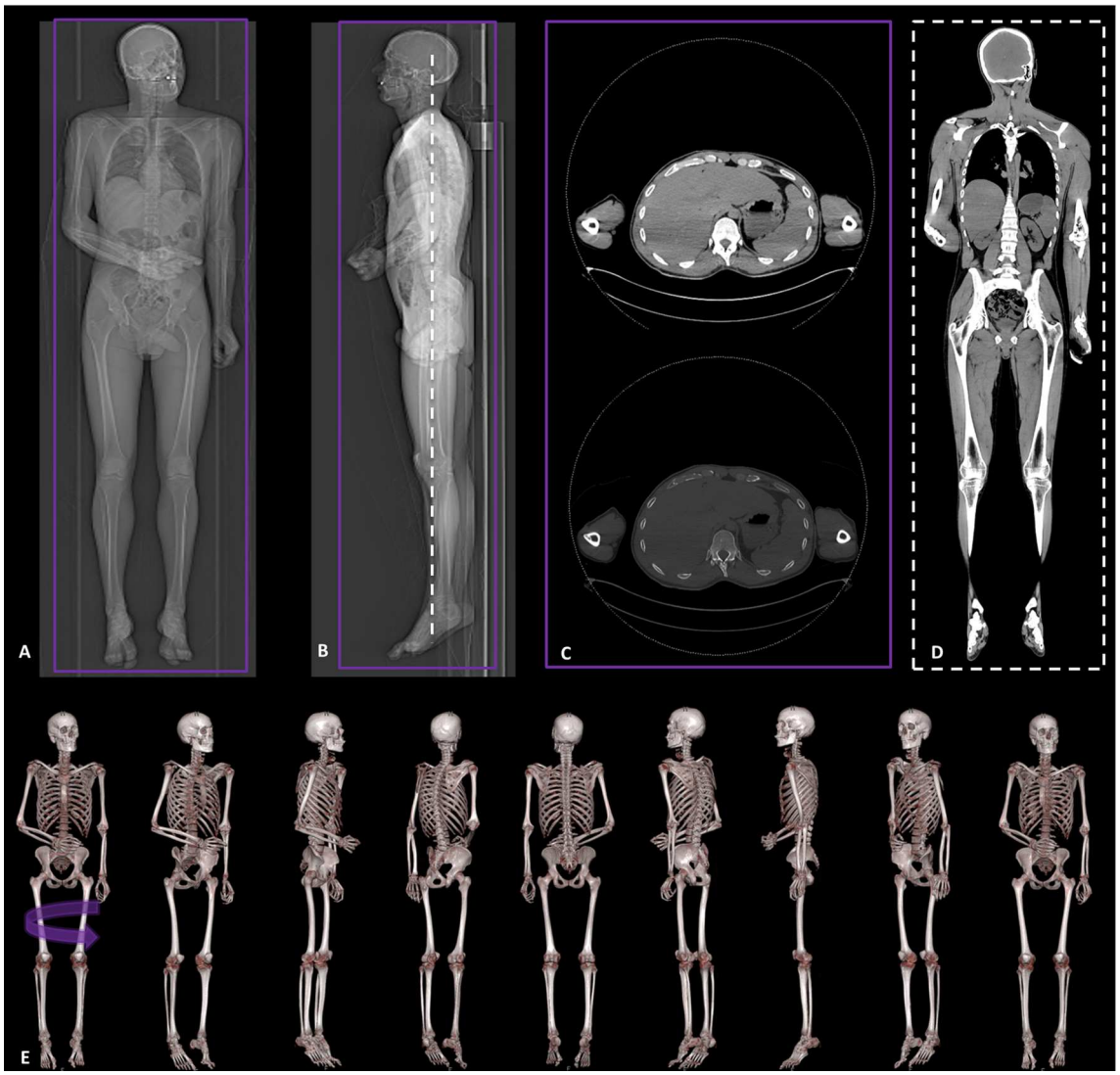

Fig. 9 *Step 1* Whole-body scan—"The Baseline". **a** Scout view of the whole-body PMCT in anterior-posterior orientation (eFoV marked by the *purple planning rectangle*). **b** Scout view of the whole-body PMCT in lateral orientation (eFoV marked by the *purple planning rectangle*). **c** Axial image reconstruction is calculated with a slice thickness of 2 mm, with a soft kernel in the abdominal window (*top image*) and a hard kernel in the bone window (*bottom image*). The whole body scan is reconstructed in eFoV to include as much of the extremities as possible. The field of view is indicated by the *purple planning rectangle* on images **a**, **b**. **d**: Coronal whole-body reconstruction in a soft kernel, with an abdominal window with a slice thickness of 3 mm. **e** VRT with a 360° video of the skeletal findings is helpful in obtaining a quick overview of the extent of bony destruction (e.g., determining the side of impact in a case of a traffic accident)

shoulder girdle with the soft tissue above the AC joints (acromio-clavicular joints; to depict pathologies, such as hematomas, along the vascular sheaths of the supra-aortal branches and the clavicle). Distally, the scan range should be terminated below the pubic bone. The reference is 400mAs with automated dose modulation. The imaging parameters for the 2 axial stacks are defined as follows: an SL of 1 mm; and an increment of 0.6 mm, in a pulmonary window with a sharp kernel (B60) and in an abdominal window with a soft kernel (B30). The osseous findings should be read out in the sharp kernel while switching from the pulmonary window to the bone window, to avoid overlooking subtle findings, such as buckle-rib fractures [64].

The torso requires the most extensive reconstructions: an axial stack is first calculated with thick slices in an abdominal window with a soft kernel (B30) (SL 5 mm, increment 3 mm) for a fast work-up and a better signal-to-noise ratio. If elevation of the arms is not feasible, separate reconstructions of the torso should still be performed after scanning, using the same parameters but an increased dose (Fig. 14).

All of the following image reconstructions are calculated with an SL of 1.5 mm and an increment of 1 mm in a sharp

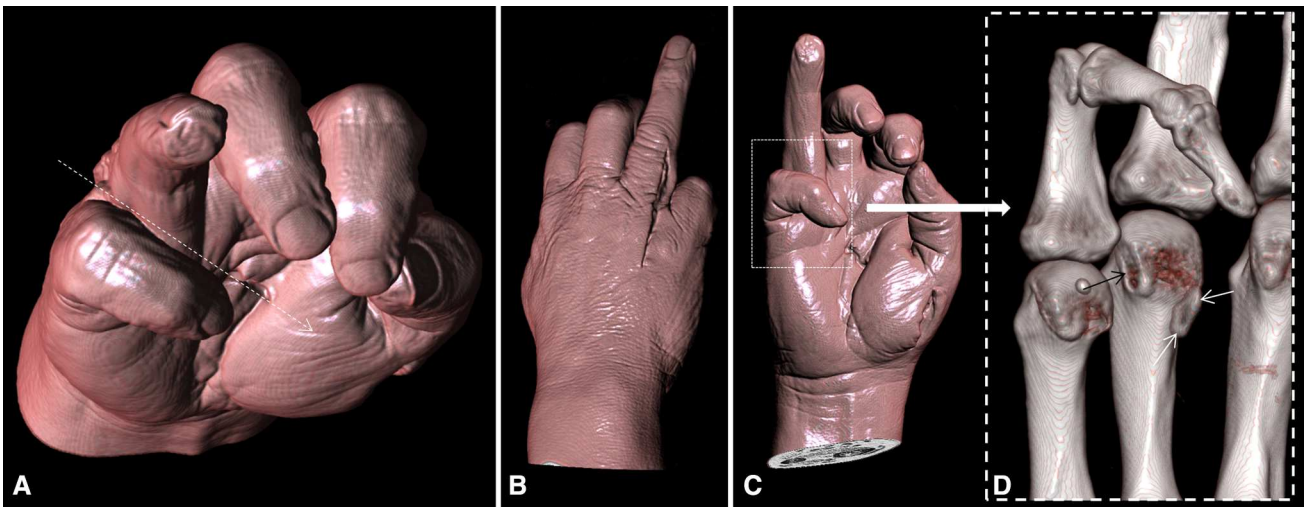

Fig. 10 **a** VRT of the right hand displaying extensive defensive injuries in a case of a homicidal stabbing. The *white dotted arrow* indicates the direction of a stabbing action from the dorsum of the hand to the palm. **b** VRT of the back of the right hand showing the stabbing wound between the 4th and 5th phalanx, corresponding to the inflicted wound in image **a**. **c** VRT of the palm of the right hand, displaying several other stab wounds in the soft tissue. The *dotted white square* indicates the area magnified on image **d**. The fingers are bent in this position due to rigor mortis. **d** VRT of the metacarpal and proximal phalanx of the 4th and 5th finger of the right hand. This inflicted injury corresponds to the wound channel shown in images **a**, **b**. Note the small, dislocated osseous flake (*white arrows*) from the ulnar caput of the 4th metacarpal (*black arrow*). This extra scan of the hand was required to depict the defensive injuries in properly court and to rule out any small metallic fragments that had splintered from the weapon used in the crime that would need to be recovered during autopsy

kernel (B70) with a bone window. Again, similar to the axial 3-dimensional reconstructed images of the cervical spine, a small FoV is applied to the thoracic and lumbar spine. The axial slices are aligned symmetrically to the intervertebral disks, and they include the transverse process on both sides. The sagittally aligned reconstruction is orthogradely centered to the middle of the vertebrae and is aligned with the course of the thoracic and lumbar spine, including the sacrum and os coccygis. In cases of extensive scoliosis or vertebral dissociation due to trauma, the thoracic spine and an extra lumbar sagittal stack might require splitting. The coronal images include the thoracic and lumbar spine and are centered symmetrically on the middle of the vertebra, including the complete vertebral body with the spinous process. The sacrum and os coccygis are included in the pelvic reconstruction. Thus, an additional coronal reconstruction, with a small FoV of the pelvis, is added. The FoV encompasses the complete, symmetrically aligned pelvis: the sacrum, the os coccygis, the symphysis, the iliac and pubic bones and both femoral heads. For a precise report of resuscitation-related injuries to the sternum, a sagittal reconstruction is calculated, with a small FoV centered on the middle of the manubrium, including both lateral sides of the costosternal transition to the ribs that proximally extends to the sternoclavicular joints (Fig. 14).

Special reconstruction parameters

For cases that feature dense foreign material, such as projectiles, general metallic fragments, prostheses, and osteosyntheses or even dental fillings (gold, amalgam), an extended CT scale (not to be confused with an extended FoV) is advisable to facilitate material differentiation. The maximum width of the HU scale in a standard setting is −1,024 to +3,071 HU, which is usually sufficient for clinical cases. In a forensic setting, a larger, extended HU width is favorable and be obtained by multiplying the HU increment by a factor of 10 (−10,240 to +30,710). However, not every CT scanner is equipped with this unique feature (activated simply by checking the dedicated box on the CT reconstruction control panel under the reconstruction section), and this fact should be taken into account when considering the purchase of a new or used device for forensic-radiological purposes [65–68].

In addition, badly decomposed bodies can present with vast gas accumulations that are distributed depending on the position in the whole body [38]. The window might need to be adjusted for proper image analysis, and using a medium soft kernel for image reconstruction might be indicated for a better reporting [37, 38, 69–71].

Whole-body PMCT (<16 multidetector CT)

With dated scanners, the whole body often cannot be scanned in a single pass because the radiation source, namely the X-ray tube, was not designed to cover whole-body scans, especially not repeatedly. However, so-called outdated scanners are not necessarily precluded from forensic use. For example, although a 6-slice scanner might

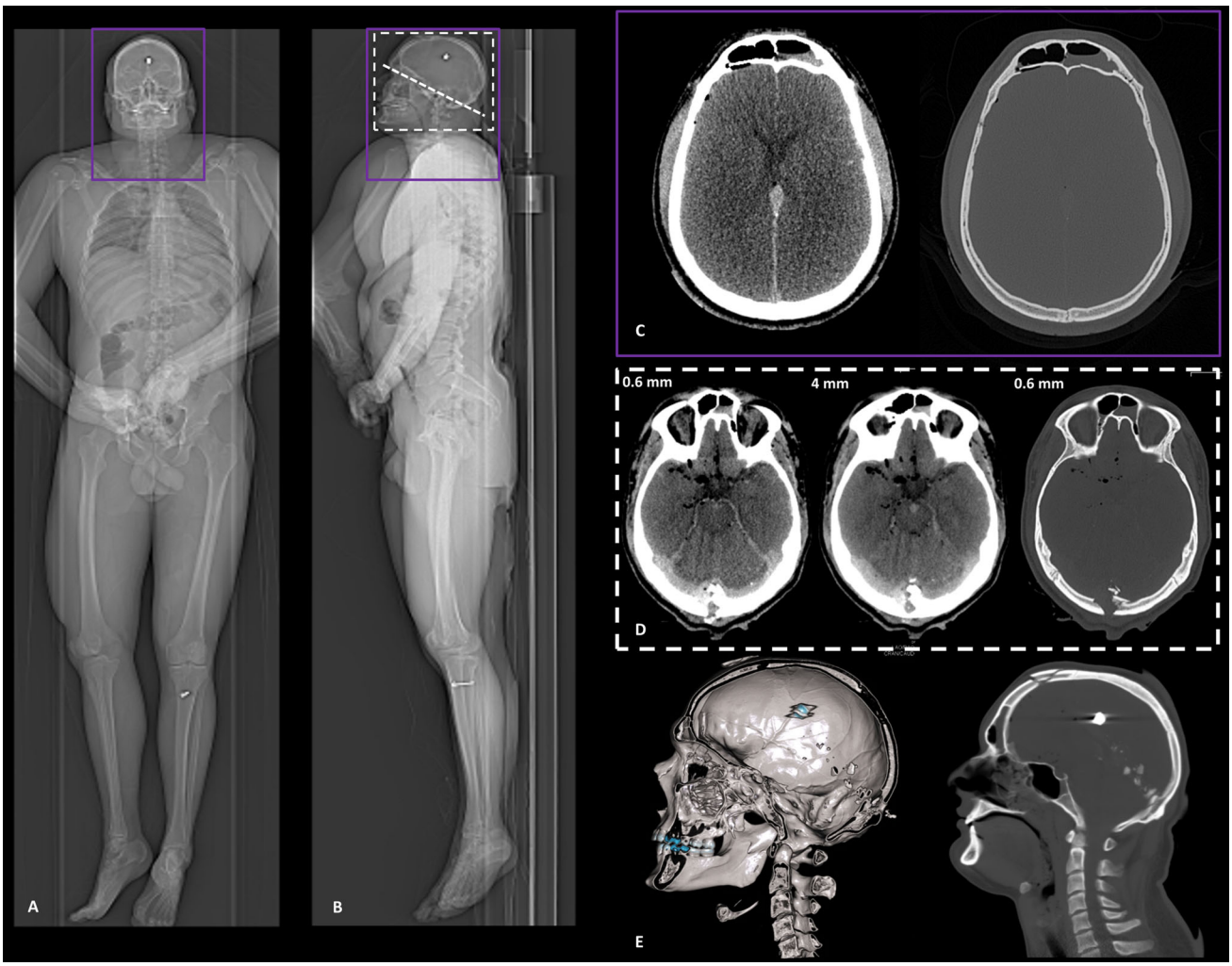

Fig. 11 *Step 2* Head and neck scan. **a** Scout view of the head and neck PMCT in anterior-posterior orientation (the small adjusted FoV is marked by the *purple planning rectangle*). **b** Scout view of the head and neck PMCT in lateral orientation (the small adjusted FoV is marked by the *purple planning rectangle*, and the *white square* indicates the orbito-meatal reconstruction FoV). **c** The axial slices (corresponding to the *purple planning rectangle*) are reconstructed in a small field of view, including the head and neck. Both axial data sets are acquired in a cerebral window with a soft kernel and a bone window with a hard kernel in 0.6 mm slice thickness. Note the typical postmortem loss of cortico-medullary differentiation between the *white* and *gray* matter and the intracranial hemorrhage. **d** Symmetrically and orbito-meatally aligned (*dotted white line*) reconstruction of the head (corresponding to the *white square* on image **b**) is calculated in a cerebral window in a soft kernel in 4 and 0.6 mm slice thicknesses, respectively. An additional stack in an osseous window with a sharp kernel, in 0.6 mm slice thickness, is performed. Note the typical inward beveling of the entry wound of a gunshot to the head (best seen on the bone window) and the pneumencephalon. **e** This image displays an optional VRT (*left image*) with a cut plane along the trajectory of a gunshot wound to the head. The entry wound is in the median occipital location, with a corresponding defect in the front parietal bone. However, this case shows a lodged projectile (*colored in light blue*) along the wound channel that did not perforate but that penetrated. Typical findings include the scattered osseous fragments along the trajectory, with little metallic abrasion of the projectile (*right image*, thick multiplanar reconstruction)

be considered outdated, these devices can offer a low-priced alternative to newer clinical scanners for forensic purposes. These refurbished CT suites currently cost the same as fluoroscopy units. Financial considerations are the primary incentive in forensics for buying a dated multi-detector CT scanner, rather than a brand-new potent CT that exceeds 16 slices.

Unfortunately, the scan length of such outdated machines (1,500 mm) is usually restricted due to a short table run, which does not cover the lower extremities. To include these body parts in the whole-body scan, the body must be rotated 180° on the CT couch, from the cranio-caudal position to the caudo-cranial position. Another drawback of less powerful scanners is the cooling time because these machines often still use air-cooling and not water-cooling. This complication results in longer scan times to cover the whole body. To reduce the waiting time for cooling, short scan ranges should be planned, i.e., the head, neck, thorax,

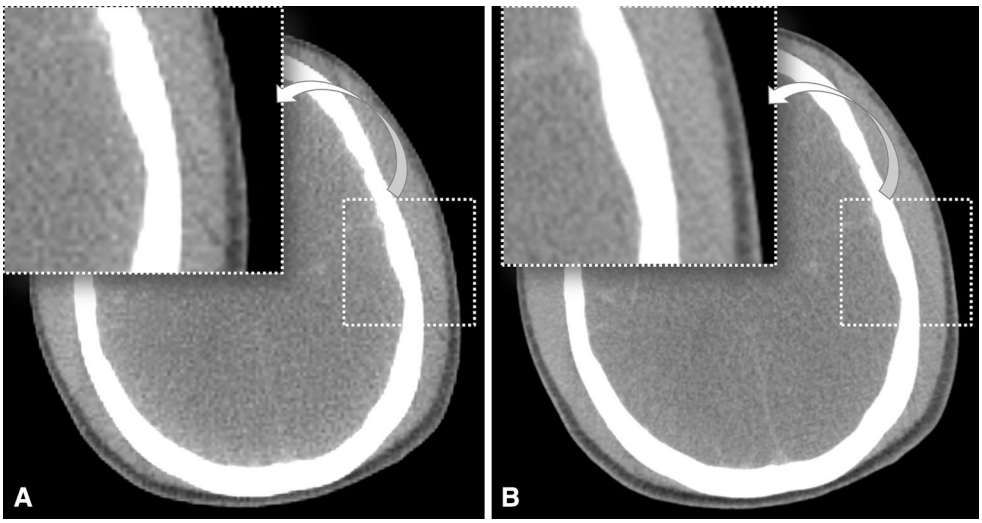

Fig. 12 **a** Axial slices are reconstructed in a large field of view. Note the decreased image quality, compared to image reconstruction with a small FoV (**b**). **b** Small, adjusted FoV with a maximum of 300 mm for better image quality

abdomen, proximal lower extremities, and distal lower extremities should all be scanned separately [38]. Moreover, the planned scan areas should not overlap (but should be exactly planned without any loss of information between the adjacent scan ranges) to later compose a virtual whole-body scan by merging the scanned volume rendered images into a single complete full-body scan (using image processing software). If the separate scan has the same FoV and center, the images can be composed directly at the CT workstation. Pitch factor alterations result in obligatory manual adaption of the milliampere level with older scanners, in which they differ from newer scanners. With current CT scanners, the milliampere level is automatically adjusted if the pitch factor increases [72].

Moreover, the bore diameter frequently does not exceed 70 cm, which concomitantly reduces the image information of the soft tissue and the extremities in cases of obese or rigidly positioned bodies, of which a CT scan is almost impossible.

The scanning protocol should be adjusted from the above-described recommended protocol by slightly thickening the SL to 2–3 mm (and eventually up to 5 mm), halving the SL increment, increasing the pitch, lowering the milliampere level and occasionally changing the kilovolt level to only 100 or even 80, if necessary. These changes are justified by the aforementioned technical limitations. The torso should still be scanned once with lowered arms and again with elevated arms to reduce artifacts.

Add-on to PMCT protocol: high-resolution scans

Dental

Dental identification requires scanning parameters with high spatial resolution to reconstruct precise images from the CT data set for antemortem X-ray comparison [73, 74]. The planning on the magnified scout view includes the base of the maxillary sinus, and it ends distally at the mandible. The FoV (usually approximately 240 mm) terminates behind the temporo-mandibular joints and includes the complete maxilla and mandible. Doing so reliably includes the root canals with their distinct morphology, in addition to the teeth and their potential dental work for later identification (Fig. 15). The imaging parameters are defined as follows: 120 kV, a reference of 800mAs, a pitch factor of 0.35, a rotation time of 1 s, an SL of 0.4 mm, and an increment of 0.2 mm with a hard kernel (U70) in a dental window. For extended CT scale reconstructions, the provided reconstruction parameters should simply be activated, and the box for the extended CT scale should be clicked (as described above). Only 1 aligned reconstruction in an axial plane must be made with the 3-dimensional reconstruction tool. The teeth and temporo-mandibular joints should be aligned orthogonally and symmetrically. This alignment is usually sufficient for single-tooth antemortem X-ray comparison. However, a curved multiplanar reconstruction is required to create a "virtual" orthopantomogram (OPT), similar to antemortem OPTs of the complete jaw (Fig. 15).

Larynx

Laryngeal scans are necessary when trauma to the neck is suspected, e.g., strangulation [75]. The images are always reported on axial slices, but the complex anatomy of the hyoid bone and the thyroid cartilage, with its variable anatomy, frequent anomalies and age-dependent stages of ossification, especially of the cornu, call for the 3-dimensional volume rendering technique (VRT)

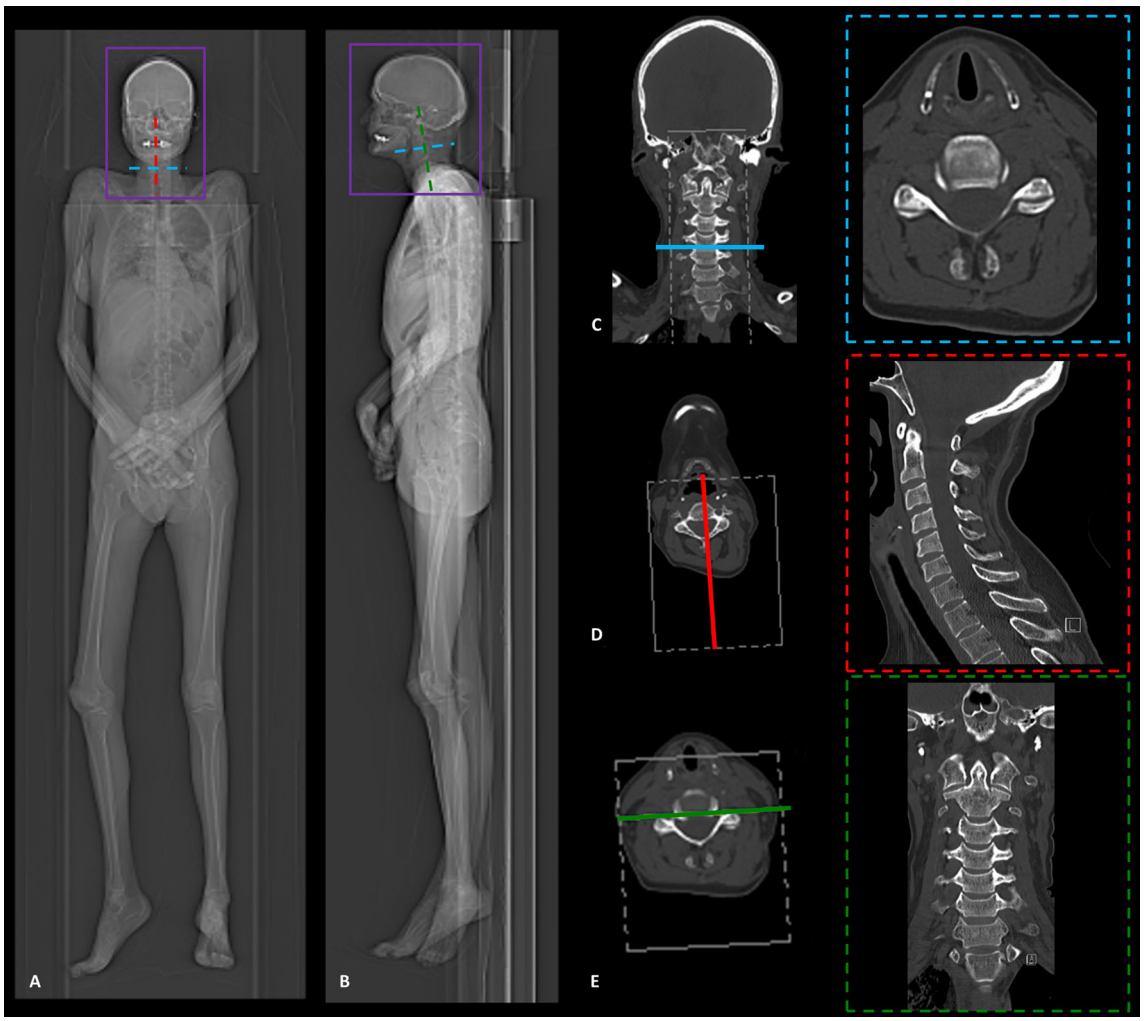

Fig. 13 *Step 2* Head and neck scan. **a** Scout view of the head and neck PMCT in anterior-posterior orientation (the small adjusted FoV is marked by the *purple planning rectangle*). **b** Scout view of the head and neck PMCT in lateral orientation (the small adjusted FoV is marked by the *purple planning rectangle*). The *blue lines* in images **a**, **b** indicate the orientation of the axial reconstruction (**c**), the *red line* indicates the orientation of the sagittal reconstruction (**d**), and the *green line* indicates the orientation of the coronal reconstruction (**e**). **c** Axial, 3-dimensional, correctly aligned reconstruction of the cervical spine (*marked in blue*). **d** Sagittal, 3-dimensional, correctly aligned reconstruction of the cervical spine (*marked in red*). **e** Coronal, 3-dimensional, correctly aligned reconstruction of the cervical spine (*marked in green*). Images **c**–**e** are calculated in 1.5 mm slice thickness in a bone window with a sharp kernel

(Fig. 16) [38, 75]. VRT allows for the easily understandable display of buckled or even fractured parts of the larynx, in correlation with the axial slices. The imaging parameters are similar to the dental scan and are reconstructed with a medium soft kernel (U40) in a bony window. The medium soft kernel is necessary to reduce the noise for later VRT. Using a sharp kernel will result in too much noise.

Again, the FoV must be adjusted only to include the complete hyoid bone, the thyroid and the cricoid cartilage. When the images are acquired non-symmetrically, an additional 3-dimensional axial reconstruction might be necessary.

General PMCTA protocol

The PMCTA procedure has already been precisely described in the recent literature [45–52]. Thus, this section only concerns the actual scanning parameters of PMCTA (Table 3).

A scout view must be obtained from the head to the middle of the upper parts of the lower extremities (which should always include the mostly femoral cannulations for contrast administration). Again, the proper positioning of the body is crucial. Other than in the described unenhanced protocol, a kilovolt level of only 100 is used for better iodine contrast. The automated dose modulation is not used

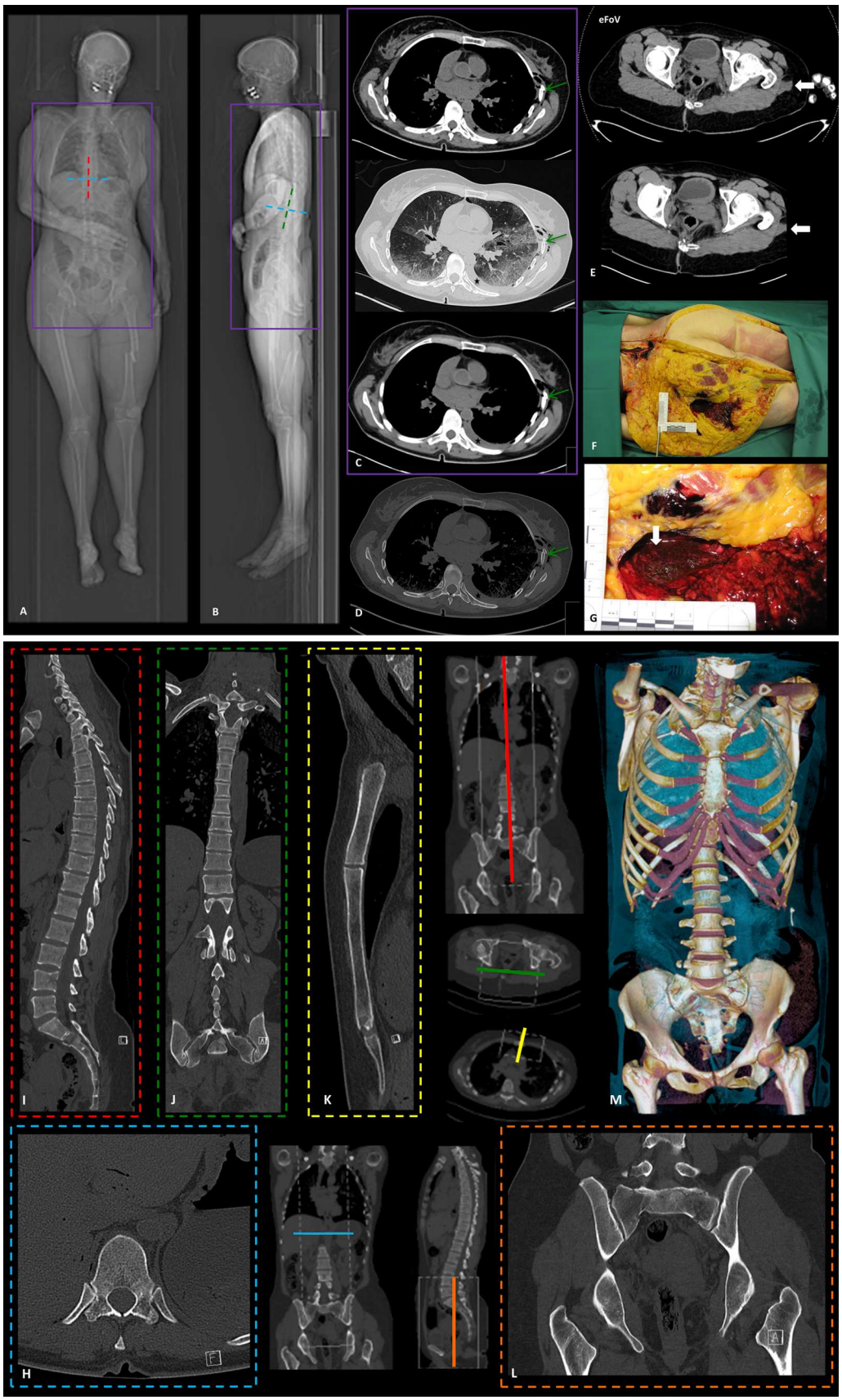
eFoV
A
B
C
D
E
F
G
H
I
J
K
L
M

◀**Fig. 14** *Step 3* Thorax and abdomen scan. **a** Scout view of the thorax and abdomen PMCT in anterior-posterior orientation (the adjusted FoV is marked by the *purple planning rectangle*). **b** Scout view of the thorax and abdomen PMCT in lateral orientation (the adjusted FoV is marked by the *purple planning rectangle*). Note that the initial topogram (images **a**, **b**) is usually not repeated; therefore, the arms are still lowered on the scout view image, although they had been raised. In images **a**, **b**, the *blue lines* indicate the orientation of the axial reconstruction (**h**), the *red line* indicates the sagittal reconstruction (**i**), and the *green line* indicates the coronal reconstruction (**j**) of the thoracolumbar spine. **c** Top image: abdominal window with a soft kernel in 1 mm slice thickness (adjusted FoV and elevated arms). Middle image: pulmonary window with a sharp kernel in 1 mm slice thickness (adjusted FoV and elevated arms). *Bottom image* abdominal window with a soft kernel in thick slices (3 mm), with a better signal-to noise ratio. Note the slight left-sided hemithorax (*black asterisk*) with small lung lacerations and pneumothorax due to left-sided traumatic impact of the thorax (the *green arrow* exemplarily marks the fractured ribs) after the pedestrian was hit by a tram. **d** The osseous findings should be read out in a sharp kernel while switching from the pulmonary window (middle image on **c**) to the bone window. **e** *Top image* eFoV scan of the whole body shows the complete soft tissue and displays a Morel-Lavallée lesion (closed degloving injury, *bold white arrow*) in loco typico on the left, due to the shearing force of subcutaneous tissue away from the underlying fascia. The lesion fills with fluid, in this case predominantly blood. This finding hints at a traumatic impact on the left side of the body. *Bottom image* separate scan of the thorax and abdomen with the trade-off of loss of information of parts of the soft tissue (*bold white arrow*) but with the desired advantage of better image quality. The investigator should therefore always read the whole-body scan, as well as the separate scans, to obtain the complete picture. **f** Overview photograph of the left thigh, displaying the Morel-Lavallée lesion (*bold white arrow*) during soft tissue dissection. The findings corresponded to the imaging. **g** Detail of image **f**. Macroscopic photograph of the Morel-Lavallée lesion filled with blood (*bold white arrow*). **h** Axial, 3-dimensional, correctly aligned reconstruction of the thoraco-lumbar spine (*marked in blue*, refer to images **a**, **b**). **i** Sagittal, 3-dimensional, correctly aligned reconstruction of the thoraco-lumbar spine (*marked in red* refer to image **a**). **j** Coronal, 3-dimensional, correctly aligned reconstruction of the thoraco-lumbar spine (*marked in green*, refer to image **b**). **k** Sagittal, strictly medially aligned reconstruction of the sternum (*marked in yellow*). **l** Coronal reconstruction of the pelvis (*marked in orange*). Note the longitudinal fractures of the massa lateralis of the sacrum and the dislocated fracture of the right transverse process of the 5th lumbar vertebra. Images **f–j** are calculated in 1.5 mm slice thickness in a bone window with a sharp kernel. **m** Optional VRT with easily understandable visualization of the traumatic impact on the left rib cage, the fractures of the sacrum and transverse process and the dislocated comminuted fracture of the coccygeal bone

for PMCTA. The following settings are effective: 350mAs; a pitch factor of 0.35; and a rotation time of 0.5 s.

Usually, arterial injection is the first "contrast phase" that should be scanned after administration, except when venous pathologies (e.g., laceration of the caval vein) or pulmonary thrombembolisms are strongly suspected. In these cases, venous injection should precede arterial injection to display the pulmonary trunk better. After the required contrast volume is administered, the scan should be performed as quickly as possible, while still slowly injecting small volumes during the scans to maintain the distension of the vascular lumen.

If the planning of the scan or adjustments of the arms takes too long, more contrast media mixture (between 500 ml and 1000 ml) can be injected according to the habitus.

Step 1: Arterial PMCTA

A spiral is scanned from the head to the thighs (including the femoral accesses) with lowered arms. The head and neck are then separately axially reconstructed (using the 3-dimensional reconstruction tool with correct alignments) from the raw data, with an SL of 1 mm and an increment of 0.5 mm in a medium soft kernel (B26) in an angio window. The complete data set of the head and neck, thorax and abdomen (including the upper extremities) is reconstructed in a medium soft (B26) and sharp heart view (B46) kernel, with both a CT angio window with the same parameters as the head and neck in an eFoV (Fig. 17).

Step 2: Arterial PMCTA

The upper extremities then must be elevated immediately to improve the image quality of the torso. This scan only includes the thorax and abdomen, with the same imaging and reconstruction parameters as mentioned above (Fig. 17). If the right coronary artery or the heart chambers are insufficiently filled, the body should be turned to a prone position to be re-injected prior to scanning. In this manner, the problem of gravity can be overcome, and even the right coronary artery should be nicely distended with contrast media mixture (if no pathology or cruor is present).

Step 3: Venous PMCTA

The arms should remain elevated, and the cannulation connection should be changed from the arterial to the venous injection site. The next scan is performed directly after injection of the contrast media mixture. The parameters are similar to those of step 2 (Fig. 17).

Step 4: Venous PMCTA

The upper extremities should now be lowered again for a scan similar to step 1, to obtain proper images of the head (Fig. 17).

Clearly, additional separate scans can be supplemented, e.g., focused scanning of the hand and wrist in the case of an inflicted wound to the radial arteries with extravasation

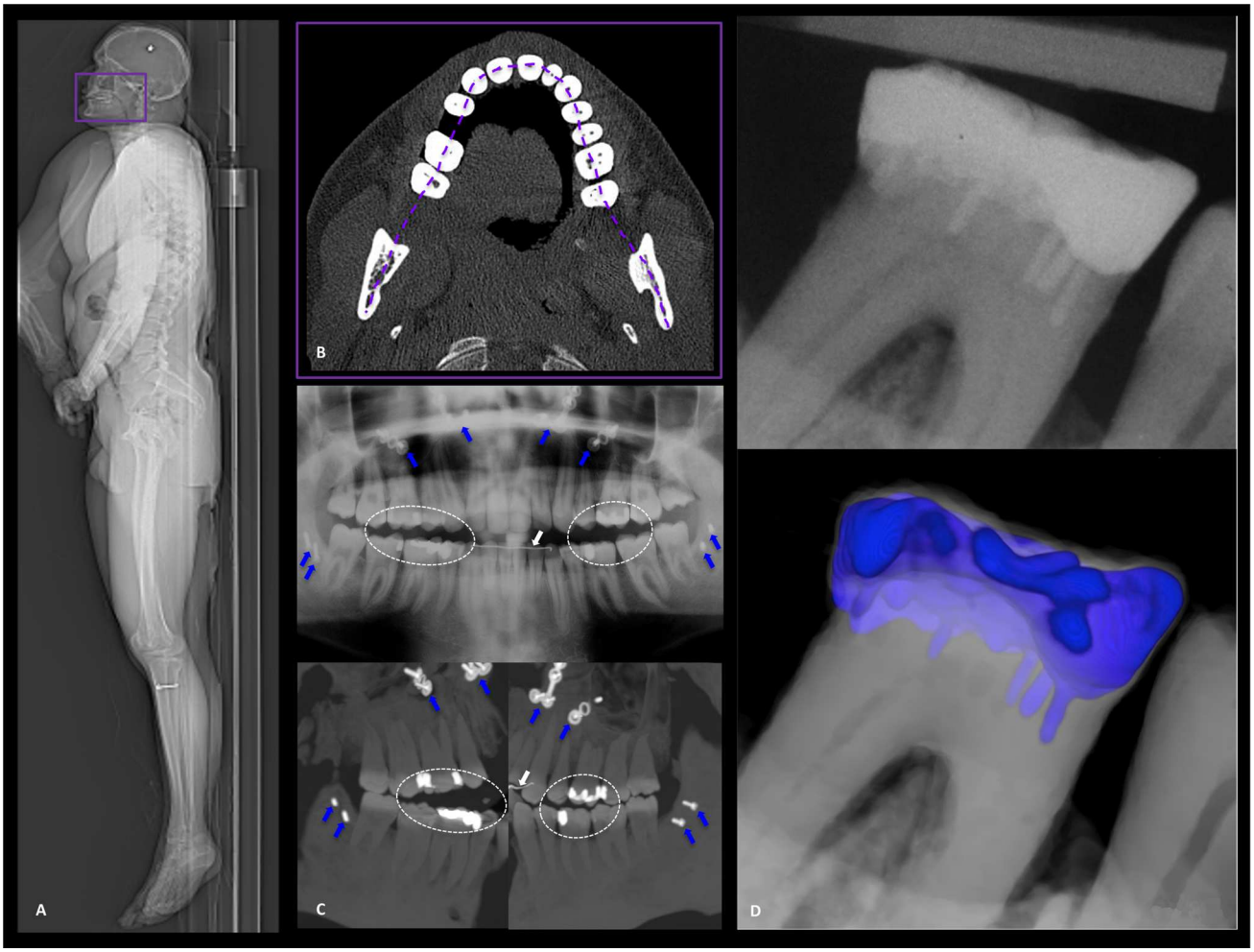

Fig. 15 Add-on to PMCT protocol: Dental. **a** Scout view of the dental PMCT in lateral orientation (the small, adjusted FoV is marked by the *purple planning rectangle*). **b** Axially aligned slices in a hard kernel and dental window, with high resolution and a slice thickness of 0.4 mm. This image displays the curved multiplanar reconstruction that is used to create a "virtual" orthopantomogram (OPT), similar to antemortem OPTs of the complete jaw. **c** Upper row image: antemortem OPT depicting extensive osteosynthetic work in the maxilla and mandible (indicated by the *bold blue arrows*), dental retainer dorsal to the front teeth of the jaw (*bold white arrow*) and dental fillings (*white circle*). *Lower row image, left* postmortem curved MPR of the right side of the jaw. *Lower row image, right* postmortem curved MPR of the left side of the jaw. The postmortem MPR displays a perfect match for the antemortem OPT, showing the exact same osteosynthetic work (*blue bold arrows*), a part of the retainer (*bold white arrow*) and the distinct shape of the dental fillings (*white circle*). Dental identification could clearly have been made by this postmortem scan, creating a "virtual" OPT. **d** *Upper image* antemortem X-ray of a single molar. *Bottom image* postmortem volume-rendered reconstruction with excellent depiction of the dental work (*color-coded in blue*); the distinct morphology could easily be used for identification purposes

from the vascular injury or focused scanning of the lower extremities in cases such as a shot through the femoral bone and adjacent vasculature.

General pediatric PMCT protocol

Imaging of a pediatric collective requires an adjusted protocol due to the smaller scanning subject and can be adjusted as follows [76, 77]: the body preparation and scout view are similar to the adult protocol, employing a whole-body scan with lowered upper extremities. Table 4 summarizes the comprehensive pediatric PMCT protocol.

Step 1: Whole-body scan

In infants and neonates, the tube voltage in all scans is 120 kV (can be increased to 140 kV in neonates) with automated dose modulation (the reference is 1000mAs for the whole-body scan). If the scanner does not allow for such a high reference level, or if it is not equipped with automated dose modulation, the protocol should be tailored

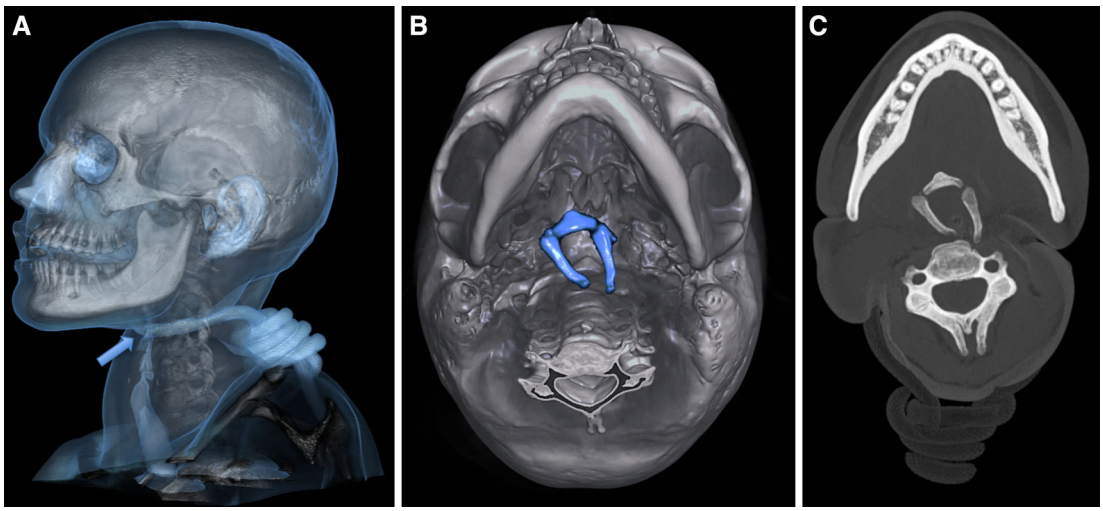

Fig. 16 Add-on to PMCT protocol: Larynx. **a** VRT of the head and neck, displaying a suicide with typical strangulation in a case of incomplete hanging. Note the narrowing of the airways (*blue arrow*), leading to suffocation during the course of strangulation. **b** Virtual combination of the VRT of the skull, caudo-cranial view with a high-resolution scan of the larynx (in this case, only the hyoid bone). The hyoid bone presents with severe deformation and displacement due to the single-rotation strangulation tool. Both greater cornu are fractured. **c** MIP (maximum intensity projection) of the hyoid bone, displaying severe narrowing of the airways and dislocation of the larynx

Table 3 Comprehensive PMCTA protocol

Region	Field of View	Orientation	Kernel	Window	I (mm)	SL (mm)
PMCTA protocol						
Step 1: Arterial PMCTA (arms next to the body)						
Head	Max. 300 mm	Axial, 3D	Medium soft (B26)	Angio	0.5	1
Head to pelvis	eFoV	Axial	Medium soft (B26)	Angio	0.5	1
Head to pelvis	eFoV	Axial	Sharp heart (B46)	Angio	0.5	1
Step 2: Arterial PMCTA (arms elevated)						
Thorax/abdomen	Max. 500 mm	Axial	Medium soft (B26)	Angio	0.5	1
Thorax/abdomen	Max. 500 mm	Axial	Sharp heart (B46)	Angio	0.5	1
Step 3: Venous PMCTA (arms elevated)						
Thorax/abdomen	Max. 500 mm	Axial	Medium soft (B26)	Angio	0.5	1
Thorax/abdomen	Max. 500 mm	Axial	Sharp heart (B46)	Angio	0.5	1
Step 4: Venous PMCTA (arms next to the body)						
Head	Max. 300 mm	Axial, 3D	Medium soft (B26)	Angio	0.5	1
Head to pelvis	eFoV	Axial	Medium soft (B26)	Angio	0.5	1
Head to pelvis	eFoV	Axial	Sharp heart (B46)	Angio	0.5	1

eFoV extended field of view, *I* increment, *SL* slice thickness, *3D* 3-dimensional, angulated reconstruction

to 120 kV and 250mAs. The rotation time is 0.5 s with a pitch of 0.6. The scan range should include the whole body, from the vertex to the toes.

The axial images are reconstructed with a SL of 0.6 mm (increment 0.4 mm) in a medium soft kernel (B25) with a baby abdominal window and in a medium sharp kernel (B50) in a bony window. The FoV must be adjusted (neonates, e.g., 240 mm) to include the extremities.

Step 2: Head and neck

The whole-body scan is then followed by a separate head and neck scan. The tube voltage remains unchanged, but the reference is increased to 2,000mAs to obtain quality images of the head. The rotation time, SL and increment are the same as in step 1. The pitch factor is changed to 0.35. Axial images (including the head and the neck, as

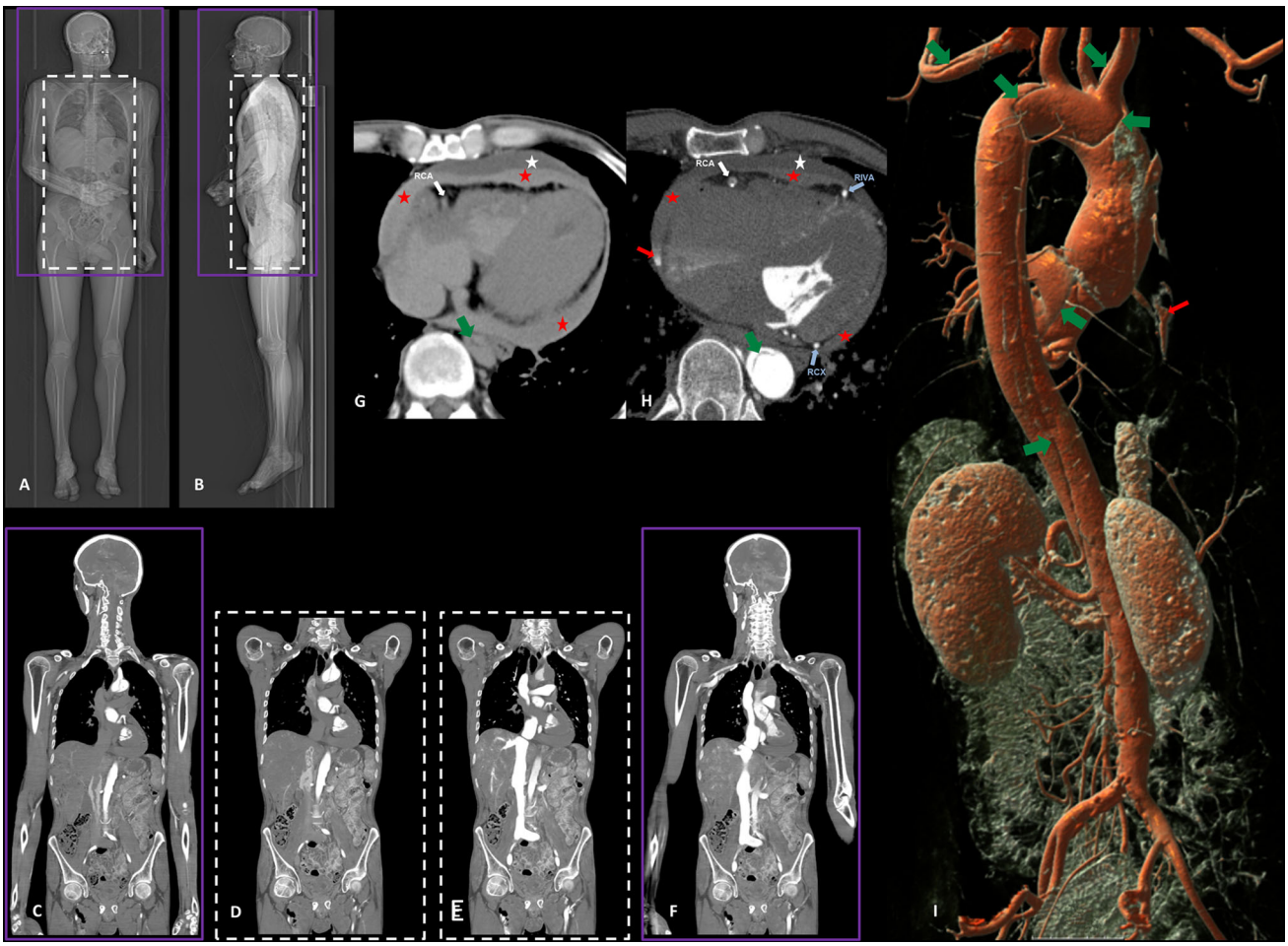

Fig. 17 General PMCTA protocol. **a** Scout view of the PMCTA in anterior-posterior orientation (eFoV is marked by the *purple planning rectangle*; the adjusted FoV is marked by the white dotted rectangle). **b** Scout view of the PMCTA in lateral orientation (eFoV is marked by the *purple planning rectangle*; the adjusted FoV is marked by the *white dotted rectangle*). **c** *Step 1* Arterial PMCTA—arms lowered. The scan range includes the region from the head to the thighs (including the femoral access) and is calculated in an eFoV with a medium soft and sharp heart view kernel, both in an angio window. The head and neck are calculated separately from this spiral (not displayed in the figure) in a medium soft kernel and with an angio window in a small FoV. **d** *Step 2* Arterial PMCTA—arms raised. This scan includes only the thorax and abdomen. For better image quality, the FoV is adjusted, and the image is reconstructed, similar to step 1. **e** *Step 3* Venous PMCTA—arms elevated. This scan is similar to step 2. Only the injection site has changed from arterial to venous. **f** *Step 4* Venous PMCTA—arms lowered. This scan is similar to step 1. The injection remains in the venous system. **g** Axial slice with depiction of the heart on unenhanced PMCT. A pericardial tamponade with clotted blood encircles the heart (*red asterisk*), creating a so-called "armored heart". The clot around the heart suggests slow hemorrhage into the pericardial sac as the blood had time to coagulate, as well as sediment. Small serous components are detectable next to the clot (*white asterisk*). The collapsed aorta suggests the subtle finding of an intimal flap (*bold green arrow*) on unenhanced imaging. **h** Axial slice with depiction of the heart on arterial PMCTA. Contrary to the unenhanced scan in **g**, the coronaries are distinguishable, and the aorta is distended after arterial injection. The dissection membrane is easily detectable (*bold green arrow*). PMCTA reveals a slight extravasation of the contrast media mixture into the hemopericardium (*red arrow*), which corresponds to the finding of an armored heart. **i** VRT of the aorta with posterior view. PMCTA displays the extent of the Stanford type A dissection into the supra-aortal branches, down to the abdominal aorta (dissection marked by *green bold arrows*). The *red arrow* indicates extravasation of contrast media mixture into the pericardial sac. Note the enhancement of both kidneys and of the intestinal mucosa due to PMCTA

well as the 1st thoracic vertebra) are reconstructed in a medium soft (H31) kernel with a baby brain window and a medium sharp (H50) kernel with a bony window. Both of these spirals are also calculated using the 3-dimensional multiplanar reconstruction tool with proper symmetric alignment and orbitomeatal orientation. For noise reduction, an additional similarly aligned 3-dimensional stack of the head should be calculated with a 2 mm SL and an increment of 1 mm, in a medium soft kernel (H31) with a baby brain window. The cervical spine is again calculated (similar to the adult PMCT protocol) in a small, adjusted FoV (e.g., 50 × 50 mm), with an orientation aligned to the

Table 4 Comprehensive pediatric PMCT protocol

Region	Field of View	Orientation	Kernel	Window	*I* (mm)	SL (mm)
Pediatric PMCT protocol						
Step 1: Whole-body						
Whole-body	Adjusted FoV	Axial	Soft (B25)	Baby abdominal	0.4	0.6
Whole-body	Adjusted FoV	Axial	Hard (B50)	Osteo	0.4	0.6
Step 2: Head and neck						
H & N	Small, adjusted FoV	Axial	Soft (H31)	Baby brain	0.4	0.6
H & N	Small, adjusted FoV	Axial	Hard (H50)	Osteo	0.4	0.6
Head	Small, adjusted FoV	Axial, 3D	Soft (H31)	Baby brain	1	2
Head	Small, adjusted FoV	Axial, 3D	Soft (H31)	Baby brain	0.4	0.6
Head	Small, adjusted FoV	Axial, 3D	Hard (H50)	Osteo	0.4	0.6
C-spine	Small, adjusted FoV	Axial, 3D	Hard (H50)	Osteo	0.4	0.6
C-spine	Small, adjusted FoV	Coronal, 3D	Hard (H50)	Osteo	0.4	0.6
C-spine	Small, adjusted FoV	Sagittal, 3D	Hard (H50)	Osteo	0.4	0.6
Step 3: Thorax and abdomen						
Thorax/abdomen	Adjusted FoV	Axial	Soft (B25)	Abdomen	0.4	0.6
Thorax/abdomen	Adjusted FoV	Axial	Hard (B60)	Lung	0.4	0.6
T-/L-spine	Small, adjusted FoV	Axial, 3D	Hard (B50)	Osteo	0.4	0.6
T-/L-spine	Small, adjusted FoV	Sagittal, 3D	Hard (B60)	Osteo	0.4	0.6
T-/L-spine	Small, adjusted FoV	Coronal, 3D	Hard (B60)	Osteo	0.4	0.6
Pelvis	Small, adjusted FoV	Coronal, 3D	Hard (B60)	Osteo	0.4	0.6

eFoV extended field of view, *I* increment, *SL* slice thickness, *3D* 3-dimensional, angulated reconstruction, *H & N* head and neck, *C-spine* cervical spine, *T-/L-spine* thoracic and lumbar spine

facet joints on the axial plane. This FoV is centered on the ossification center of the dens and the middle of the vertebral column (FoV, e.g., 50 × 73 mm) on the sagittal plane; with coronal orientation (FoV, e.g., 50 × 63 mm), including the foramen magnum on the proximal side and the 1st thoracic vertebra on the distal side, as well as both sides of the transverse and spinous process on the posterior side. The images are reconstructed with a medium sharp kernel (H50) in a bony window with a SL of 0.6 mm and an increment of 0.4 mm.

Step 3: Thorax and abdomen

The arms should now be elevated, if possible. The rotation time and pitch remain unchanged from step 2. The reference for the torso is 800mAs. An axial spiral in a medium soft kernel (B25), with an abdomen window and a sharp kernel (B60) with a lung window, is calculated using a 0.6 mm SL and an increment of 0.4 mm. According to the reconstructions of the adult thoracic and lumbar spine, a small adjusted FoV, with symmetric orientation to the facet joints, is reconstructed in the 3-dimensional multiplanar reconstruction tool, in a medium sharp (B50) kernel with a bony window. The same settings apply for the thoracic and lumbar spine (including the os coccigys) in the coronal and sagittal orientation. The last reconstruction includes the pelvis (according to the borders of the FoV as described in the adult PMCT protocol). These images are reconstructed with a SL of 0.6 mm, an increment of 0.4 mm, and an adjusted FoV with a sharp kernel (B60) in a bony window.

The lower limbs are already included in the whole-body scanning protocol and are usually not reconstructed separately, except for special requests. Children with an approximate age older than 6 years old might already undergo the adult PMCT protocol, according to the habitus.

General pediatric PMCTA protocol

The technical settings of the pediatric PMCTA protocol are similar to those of the adult PMCTA protocol. However, cannulation of the vessels is more cumbersome, and a smaller diameter of vascular access is needed. In addition, the volume of injected contrast media mixture clearly must be adapted to the habitus of the child.

Conclusion and future directions

PMCT and even PMCTA are radiological modalities that have been adopted in morgues worldwide recently and that will certainly increase over the coming years [12–36]. In

addition, the cross-sectional method of CT will certainly supersede X-ray imaging of the deceased, which is still in use in other institutions, e.g., for the localization of bullets or the imaging of fracture patterns, which are usually performed by preparers or morgue technicians [24]. As the field of radiology continues to develop, other modalities, such as PMMR and PMMRA, will find their way into standard procedures in more than a few forensic institutions, and these modalities will require trained personnel, including radiological technicians, radiologists or radiological trained forensic pathologists. These new technologies should not be left in the hands of poorly radiological trained staff, not only with regard to image quality and standards but also regarding medico-legal requirements.

Therefore, standards must be established for postmortem imaging. A new society that was recently formed (ISFRI, the International Society of Forensic Radiology and Imaging) addresses this issue as one of its goals and to generate quality standards and curricula for forensic radiology [78]. In the future, such societies will hopefully act as a base for the further international implementation of guidelines and standards in forensic imaging.

Future directions in forensic radiology will clearly adopt even more sophisticated and interdisciplinary approaches as standard procedures in selected cases, such as molecular imaging (spectroscopy, diffusion weighted imaging), micro-CT/MR, image-guided biopsy, robot-guided biopsy, photogrammetry, and surface scanning [13, 14, 79–87]. Such procedures will intensify the need for high-quality standards. In addition, other medical disciplines, such as pathology, with clinical autopsies could even adopt imaging into their workflow to improve pathological diagnoses. This approach might even improve the quality of clinical treatment [17, 18, 88].

This article should facilitate the implementation of high-quality protocols in morgues, associated hospitals or private practices that perform forensic scans. This protocol could also facilitate proper reporting and standards similar to those for clinical scans used in courts.

Key points

1. Postmortem imaging is a new radiological subspecialty, and unlike diagnostic radiology, it does not yet have established standards.
2. Clinical and postmortem radiology differ significantly in several aspects: imaging parameters can be adjusted to maximize image quality and the indications in forensic medicine are typically different from those in clinical radiology.
3. Forensic radiology's goals are to detect the cause of death and to generate insights into the deceased's mortal circumstances.
4. This article outlines the main approach for a recommended standard protocol for postmortem cross-sectional imaging, focusing on unenhanced PMCT and PMCTA.

References

1. Baglivo M, Winklhofer S, Hatch GM, Ampanozi G, Thali MJ, Ruder TD. The rise of forensic and post-mortem radiology—analysis of the literature between the year 2000 and 2011. JOFRI. 2013;1:3–9.
2. Brogdon BG. Forensic radiology in historical perspective. In: Thali MJ, Viner M, Brogdon BG, editors. Brogdon's forensic radiology. 2nd ed. Boca Raton: CRC Press; 2010. p. 3–7.
3. O'Donnell C, Woodford N. Post-mortem radiology—a new subspeciality? Clin Radiol. 2008;63:1189–94.
4. Rutty GN, Morgan B, O'Donnell C, Leth PM, Thali M. Forensic institutes across the world place CT or MRI scanners or both into their mortuaries. J Trauma. 2008;65:493–4.
5. Wüllenweber R, Schneider V, Grumme T. A computer-tomographical examination of cranial bullet wounds (author's transl). Z Rechtsmed. 1977;80(3):227–46.
6. Levy AD, Harcke TH. Essentials of forensic imaging: a text-atlas. 1st ed. Boca Raton: CRC Press; 2010.
7. Brogdon BG, editor. Forensic radiology. 1st ed. Boca Raton: CRC Press LCC; 1998.
8. Thali MJ, Viner MD, Brogdon BG. Brogdon's forensic radiology. 2nd ed. Boca Raton: CRC Press; 2010.
9. Folio LR. Combat radiology: diagnostic imaging of blast and ballistic injuries. 1st ed. New York: Springer; 2010.
10. Burke MP. Forensic pathology of fractures and mechanisms of injury: postmortem CT scanning. 1st ed. Boca Raton: CRC Press; 2011.
11. Brogdon BG, Vogel H, McDowell JDA. Radiologic atlas of abuse, torture, terrorism, and inflicted Trauma. 1st ed. Boca Raton: CRC Press; 2003.
12. Thali MJ, Dirnhofer R, Vock P. The virtopsy approach: 3D optical and radiological scanning and reconstruction in forensic medicine. 1st ed. Boca Raton: CRC Press; 2009.
13. Thali MJ, Jackowski C, Oesterhelweg L, Ross SG, Dirnhofer R. VIRTOPSY—the Swiss virtual autopsy approach. Leg Med (Tokyo). 2007;9(2):100–4.
14. Thali MJ, Yen K, Schweitzer W, Boesch C, Ozdoba C, Schroth G, Ith M, Sonnenschein M, Doernhoefer T, Scheurer E, Plattner T, Dirnhofer R. Virtopsy a new imaging horizon in forensic pathology: virtual autopsy by postmortem multislice computed tomography (MSCT) and magnetic resonance imaging (MRI)—a feasibility study. J Forensic Sci. 2003;48:386–403.
15. The Virtopsy Project. http://www.virtopsy.com. Accessed 1 June 2013.
16. Pollanen MS, Woodford N. Virtual autopsy: time for a clinical trial. Forensic Sci Med Pathol. 2013;9(3):427–8.
17. Wichmann D, Obbelode F, Vogel H, Hoepker WW, Nierhaus A, Braune S, Sauter G, Pueschel K, Kluge S. Virtual autopsy as an alternative to traditional medical autopsy in the intensive care unit: a prospective cohort study. Ann Intern Med. 2012;156(2):123–30.
18. Westphal SE, Apitzsch J, Penzkofer T, Mahnken AH, Knüchel R. Virtual CT autopsy in clinical pathology: feasibility in clinical autopsies. Virchows Arch. 2012;461(2):211–9.
19. Scandurra I, Forsell C, Ynnerman A, Ljung P, Lundström C, Persson A. Advancing the state-of-the-art for Virtual Autopsies–initial forensic workflow study. Stud Health Technol Inform. 2010;160(Pt 1):639–43.

20. Blaauwgeers JL, van Rijn RR. Virtual autopsy–why not? Ned Tijdschr Geneeskd. 2012;156(19):A4786.
21. Persson A, Lindblom M, Jackowski C. A state-of-the-art pipeline for postmortem CT and MRI visualization: from data acquisition to interactive image interpretation at autopsy. Acta Radiol. 2011;52(5):522–36.
22. Levy AD, Abbott RM, Mallak CT, Getz JM, Harcke HT, Champion HR, Pearse LA. Virtual autopsy: preliminary experience in high-velocity gunshot wound victims. Radiology. 2006;240(2):522–8.
23. Levy AD, Harcke HT, Getz JM, Mallak CT, Caruso JL, Pearse L, Frazier AA, Galvin JR. Virtual autopsy: two- and three-dimensional multidetector CT findings in drowning with autopsy comparison. Radiology. 2007;243(3):862–8.
24. Harcke HT, Levy AD, Abbott RM, Mallak CT, Getz JM, Champion HR, Pearse L. Autopsy radiography: digital radiographs (DR) vs multidetector computed tomography (MDCT) in high-velocity gunshot-wound victims. Am J Forensic Med Pathol. 2007;28(1):13–9.
25. Daly B, Abboud S, Ali Z, Sliker C, Fowler D. Comparison of whole-body post mortem 3D CT and autopsy evaluation in accidental blunt force traumatic death using the abbreviated injury scale classification. Forensic Sci Int. 2013;225(1–3):20–6.
26. Takahashi N, Higuchi T, Shiotani M, Hirose Y, Shibuya H, Yamanouchi H, Hashidate H, Funayama K. The effectiveness of postmortem multidetector computed tomography in the detection of fatal findings related to cause of non-traumatic death in the emergency department. Eur Radiol. 2012;22(1):152–60.
27. Shiotani S, Kobayashi T, Hayakawa H, Kikuchi K, Kohno M. Postmortem pulmonary edema: a comparison between immediate and delayed postmortem computed tomography. Leg Med (Tokyo). 2011;13(3):151–5.
28. Roberts IS, Benamore RE, Benbow EW, Lee SH, Harris JN, Jackson A, Mallett S, Patankar T, Peebles C, Roobottom C, Traill ZC. Post-mortem imaging as an alternative to autopsy in the diagnosis of adult deaths: a validation study. Lancet. 2012;379:136–42.
29. O'Donnell CJ, Woodford N. Imaging the dead. Can supplement but not replace autopsy in medicolegal death investigation. BMJ. 2010;341:c7415.
30. Capuani C, Guilbeau-Frugier C, Dedouit F, Rougé D, Delisle MB, Telmon N. Forensic scientist's implication regarding medical autopsies: experience in a French university hospital (CHU Toulouse). Ann Pathol. 2013;33(2):87–92.
31. Leth PM. Computerized tomography used as a routine procedure at postmortem investigations. Am J Forensic Med Pathol. 2009;30(3):219–22.
32. Woźniak K, Gross A, Konopka T, Pohl J, Kłys M. Report from the medico-legal autopsy of the exhumed corpse of general Władysław Sikorski. Arch Med Sadowej Kryminol. 2009;59(1):15–21.
33. Bedford PJ, Oesterhelweg L. Different conditions and strategies to utilize forensic radiology in the cities of Melbourne, Australia and Berlin, Germany. Forensic Sci Med Pathol. 2013;9(3):321–6.
34. Thomsen AH, Jurik AG, Uhrenholt L, Vesterby A. An alternative approach to computerized tomography (CT) in forensic pathology. Forensic Sci Int. 2009;183(1–3):87–90.
35. Rutty GN, Brogdon G, Dedouit F, Grabherr S, Hatch GM, Jackowski C, Leth P, Persson A, Ruder TD, Shiotani S, Takahashi N, Thali MJ, Woźniak K, Yen K, Morgan B. Terminology used in publications for post-mortem cross-sectional imaging. Int J Legal Med. 2013;127(2):465–6.
36. Burton EC, Mossa-Basha M. To image or to autopsy? Ann Intern Med. 2012;156(2):158–9.
37. Christe A, Flach P, Ross S, Spendlove D, Bolliger S, Vock P, Thali MJ. Clinical radiology and postmortem imaging (Virtopsy) are not the same: specific and unspecific postmortem signs. Leg Med (Tokyo). 2010;12(5):215–22.
38. Flach PM, Ross SG, Thali MJ. Clinical and Forensic Radiology are not the same. In: Thali MJ, Viner MD, Brogdon BG, editors. Brogdon's forensic radiology. 2nd ed. Boca Raton, London, New York, Washington, DC: CRC Press, Taylor & Francis Group; 2010. p. 409–440.
39. Saukko P, Knight B, editors. Knight's forensic pathology. 3rd ed. London: Edward Arnold; 2004.
40. Gralla J, Spycher F, Pignolet C, Ozdoba C, Vock P, Hoppe H. Evaluation of a 16-MDCT scanner in an emergency department: initial clinical experience and workflow analysis. AJR. 2005;185:232–8.
41. Novelline RA, Rhea JT, Rao PM, Stuk JL. Helical CT in emergency radiology. Radiology. 1999;213:321–39.
42. Linsenmaier U, Krötz M, Häuser H, Rock C, Rieger J, Bohndorf K, Pfeifer KJ, Reiser M. Whole-body computed tomography in polytrauma: techniques and management. Eur Radiol. 2002;12:1728–40.
43. Computed Tomography (CT) Guidelines. http://www.acr.org/Quality-Safety/Standards-Guidelines/Practice-Guidelines-by-Modality/CT. Accessed 19 Apr 2013.
44. Karlo C, Gnannt R, Frauenfelder T, Leschka S, Brüesch M, Wanner GA, Alkadhi H. Whole-body CT in polytrauma patients: effect of arm positioning on thoracic and abdominal image quality. Emerg Radiol. 2011;18:285–93.
45. Ross SG, Flach PM, Thali MJ. Postmortem Angiography. In: Thali MJ, Viner MD, Brogdon BG, editors. Brogdon's forensic radiology. 2nd ed. Boca Raton, London, New York, Washington, DC: CRC Press, Taylor & Francis Group; 2010. p. 449–460.
46. Ross SG, Thali MJ, Bolliger S, Germerott T, Ruder TD, Flach PM. Sudden death after chest pain: feasibility of virtual autopsy with postmortem CT angiography and biopsy. Radiology. 2012;264(1):250–9.
47. Flach PM, Ross SG, Bolliger SA, Preiss US, Thali MJ, Spendlove D. Postmortem whole-body computed tomography angiography visualizing vascular rupture in a case of fatal car crash. Arch Pathol Lab Med. 2010;134(1):115–9.
48. Grabherr S, Djonov V, Yen K, Thali MJ, Dirnhofer R. Postmortem angiography: review of former and current methods. AJR. 2007;188:832–8.
49. Ross S, Spendlove D, Bolliger S, Christe A, Oesterhelweg L, Grabherr S, Thali MJ, Gygax E. Postmortem whole-body CT angiography: evaluation of two contrast media solutions. AJR. 2008;190(5):1380–9.
50. Jackowski C, Persson A, Thali MJ. Whole body postmortem angiography with a high viscosity contrast agent solution using poly ethylene glycol as contrast agent dissolver. J Forensic Sci. 2008;53:465–8.
51. Grabherr S, Doenz F, Steger B, Dirnhofer R, Dominguez A, Sollberger B, Gygax E, Rizzo E, Chevallier C, Meuli R, Mangin P. Multi-phase post-mortem CT angiography: development of a standardized protocol. Int J Legal Med. 2011;125(6):791–802.
52. Saunders SL, Morgan B, Raj V, Rutty GN. Post-mortem computed tomography angiography: past, present and future. Forensic Sci Med Pathol. 2011;7:271–7.
53. Ruder TD, Hatch GM, Ebert LC, Flach PM, Ross S, Ampanozi G, Thali MJ. Whole body postmortem magnetic resonance angiography. J Forensic Sci. 2012;57(3):778–82.
54. Aghayev E, Christe A, Sonnenschein M, Yen K, Jackowski C, Thali MJ, Dirnhofer R, Vock P. Postmortem imaging of blunt chest trauma using CT and MRI: comparison with autopsy. J Thorac Imaging. 2008;23(1):20–7.
55. Yen K, Lövblad KO, Scheurer E, Ozdoba C, Thali MJ, Aghayev E, Jackowski C, Anon J, Frickey N, Zwygart K, Weis J, Dirnhofer R. Post-mortem forensic neuroimaging: correlation of

MSCT and MRI findings with autopsy results. Forensic Sci Int. 2007;173(1):21–35.
56. Patriquin L, Kassarjian A, Barish M, Casserley L, O'Brien M, Andry C, Eustace S. Postmortem whole-body magnetic resonance imaging as an adjunct to autopsy: preliminary clinical experience. J Magn Reson Imaging. 2001;13(2):277–87. Erratum in: J Magn Reson Imaging 2001 May;13(5):818.
57. Ross S, Ebner L, Flach P, Brodhage R, Bolliger SA, Christe A, Thali MJ. Postmortem whole-body MRI in traumatic causes of death. AJR. 2012;199(6):1186–92.
58. Langkammer C, Krebs N, Goessler W, Scheurer E, Ebner F, Yen K, Fazekas F, Ropele S. Quantitative MR imaging of brain iron: a postmortem validation study. Radiology. 2010;257(2):455–62. Erratum in: Radiology. 2011;258(3):962.
59. Langkammer C, Schweser F, Krebs N, Deistung A, Goessler W, Scheurer E, Sommer K, Reishofer G, Yen K, Fazekas F, Ropele S, Reichenbach JR. Quantitative susceptibility mapping (QSM) as a means to measure brain iron? A post mortem validation study. Neuroimage. 2012;62(3):1593–9.
60. Scandurra I, Forsell C, Ynnerman A, Ljung P, Lundström C, Persson A. Advancing the state-of-the-art for virtual autopsies–initial forensic workflow study. Stud Health Technol Inform. 2010;160(Pt 1):639–43.
61. Germerott T, Flach PM, Furter M, Ampanozi G, Ruder TD, Thali MJ. Fatal thoracic impalement on postmortem imaging. Leg Med (Tokyo). 2011;13(2):83–6.
62. Dedouit F, Piercecchi-Marti MD, Leonetti G, Rougé D, Telmon N. Cause of internal hemorrhage determined after exhumation: report of one case. Forensic Sci Int. 2011;204(1–3):e20–3.
63. Levy AD, Harcke HT, Getz JM, Mallak CT. Multidetector computed tomography findings in deaths with severe burns. Am J Forensic Med Pathol. 2009;30(2):137–41.
64. Yang KM, Lynch M, O'Donnell C. "Buckle" rib fracture: an artifact following cardio-pulmonary resuscitation detected on postmortem CT. Leg Med (Tokyo). 2011;13(5):233–9.
65. Link TM, Berning W, Scherf S, Joosten U, Joist A, Engelke K, Daldrup-Link HE. CT of metal implants: reduction of artifacts using an extended CT scale technique. J Comput Assist Tomogr. 2000;24(1):165–72.
66. Lee MJ, Kim S, Lee SA, Song HT, Huh YM, Kim DH, Han SH, Suh JS. Overcoming artifacts from metallic orthopedic implants at high-field-strength MR imaging and multi-detector CT. RadioGraphics. 2007;27(3):791–803.
67. Bolliger SA, Oesterhelweg L, Spendlove D, Ross S, Thali MJ. Is differentiation of frequently encountered foreign bodies in corpses possible by Hounsfield density measurement? J Forensic Sci. 2009;54(5):1119–22.
68. Jackowski C, Lussi A, Classens M, Kilchoer T, Bolliger S, Aghayev E, Criste A, Dirnhofer R, Thali MJ. Extended CT scale overcomes restoration caused streak artifacts for dental identification in CT–3D color encoded automatic discrimination of dental restorations. J Comput Assist Tomogr. 2006;30(3):510–3.
69. Charlier P, Carlier R, Roffi F, Ezra J, Chaillot PF, Duchat F, Huynh-Charlier I, Lorin de la Grandmaison G. Postmortem abdominal CT: assessing normal cadaveric modifications and pathological processes. Eur J Radiol. 2012;81(4):639–47.
70. Fischer F, Grimm J, Kirchhoff C, Reiser MF, Graw M, Kirchhoff S. Postmortem 24-h interval computed tomography findings on intrahepatic gas development and changes of liver parenchyma radiopacity. Forensic Sci Int. 2012;214(1–3):118–23.
71. Singh MK, O'Donnell C, Woodford NW. Progressive gas formation in a deceased person during mortuary storage demonstrated on computed tomography. Forensic Sci Med Pathol. 2009;5(3):236–42.
72. Alkadhi H, Leschka S, Stolzmann P, Scheffel H. Wie funktioniert CT?. 1st ed. Berlin: Springer; 2011.
73. Thali MJ, Markwalder T, Jackowski C, Sonnenschein M, Dirnhofer R. Dental CT imaging as a screening tool for dental profiling: advantages and limitations. J Forensic Sci. 2006;51(1):113–9.
74. Dedouit F, Telmon N, Costagliola R, Otal P, Florence LL, Joffre F, Rougé D. New identification possibilities with postmortem multislice computed tomography. Int J Leg Med. 2007;121(6):507–10.
75. Kempter M, Ross S, Spendlove D, Flach PM, Preiss U, Thali MJ, Bolliger SA. Post-mortem imaging of laryngohyoid fractures in strangulation incidents: first results. Leg Med (Tokyo). 2009;11(6):267–71.
76. Sieswerda-Hoogendoorn T, van Rijn RR. Current techniques in postmortem imaging with specific attention to paediatric applications. Pediatr Radiol. 2010;40(2):141–52; quiz 259.
77. Fayad LM, Corl F, Fishman EK. Pediatric skeletal trauma: use of multiplanar reformatted and three-dimensional 64-Row multidetector CT in the emergency department. RadioGraphics. 2009;29:135–50.
78. International Society of Forensic Radiology and Imaging (ISFRI). http://www.isfri.com. Accessed 1 June 2013.
79. Ebert LC, Ptacek W, Naether S, Fürst M, Ross S, Buck U, Weber S, Thali M. Virtobot–a multi-functional robotic system for 3D surface scanning and automatic post mortem biopsy. Int J Med Robot. 2010;6(1):18–27.
80. Ebert LC, Thali MJ, Ross S. Getting in touch–3D printing in forensic imaging. Forensic Sci Int. 2011;211(1–3):e1–6.
81. Ebert LC, Hatch G, Ampanozi G, Thali MJ, Ross S. You can't touch this: touch-free navigation through radiological images. Surg Innov. 2012;19(3):301–7.
82. Scheurer E, Lovblad KO, Kreis R, Maier SE, Boesch C, Dirnhofer R, Yen K. Forensic application of postmortem diffusion-weighted and diffusion tensor MR imaging of the human brain in situ. AJNR. 2011;32(8):1518–24.
83. Germerott T, Preiss US, Ebert LC, Ruder TD, Ross S, Flach PM, Ampanozi G, Filograna L, Thali MJ. A new approach in virtopsy: postmortem ventilation in multislice computed tomography. Leg Med (Tokyo). 2010;12(6):276–9.
84. Germerott T, Flach PM, Preiss US, Ross SG, Thali MJ. Postmortem ventilation: a new method for improved detection of pulmonary pathologies in forensic imaging. Leg Med (Tokyo). 2012;14(5):223–8.
85. Buck U, Näther S, Braun M, Thali MJ. Virtopsy as a multi-tool approach. In: Thali MJ, Dirnhofer R, Vock P, editors. The virtopsy approach: 3D optical and radiological scanning and reconstruction in forensic medicine. 1st ed. Boca Raton: CRC Press; 2009. p. 389–432.
86. Ith M, Scheurer E, Kreis R, Thali M, Dirnhofer R, Boesch C. Estimation of the postmortem interval by means of ^{1}H MRS of decomposing brain tissue: influence of ambient temperature. NMR Biomed. 2011;24(7):791–8.
87. Scheurer E, Ith M, Dietrich D, Kreis R, Hüsler J, Dirnhofer R, Boesch C. Statistical evaluation of time-dependent metabolite concentrations: estimation of post-mortem intervals based on in situ 1H-MRS of the brain. NMR Biomed. 2005;18(3):163–72.
88. Fryer EP, Traill ZC, Benamore RE, Roberts IS. High risk medicolegal autopsies: is a full postmortem examination necessary? J Clin Pathol. 2013;66(1):1–7.